Proc. Lunar Planet. Sci. Conf. 9th (1978), p. 2825–2849.
Printed in the United States of America

Mare basalt types on the front side of the moon: A summary of spectral reflectance data

CARLÉ M. PIETERS

SN6/Geology Branch, NASA Johnson Space Center, Houston, Texas 77058

Abstract—A unit map of nearside basalt types has been prepared from all telescopic spectral reflectance data currently available for lunar soils. Four parameters were chosen (UV/VIS ratio, albedo, 1 μm band strength, 2 μm band strength) to distinguish and map each of 13 mare basalt types and three additional volcanic groups. Multispectral imagery and albedo maps were used to define unit boundaries while spectra were used to examine the 1 and 2 μm bands and calibrate and quantify the multispectral images. Although the volume of each basalt type is not known, it is clear from the unit map that only 1/3 to 1/2 of the surface basalt types are likely to be represented in the returned lunar samples. For mature lunar soils a single parameter alone does not provide chemical information, but when the four are used together, TiO_2 and in some cases FeO can be estimated. Further study of the mineralogy of unsampled lunar basalts requires precise spectra to 2.5 μm with higher spectral and spatial resolution.

I. INTRODUCTION

A large amount of spectral reflectance data exists for the lunar surface which can be used to define and characterize surface geologic units. The data currently consist of four principal types: (a) laboratory reflectance spectra of returned lunar samples (.35 to 2.5 μm, continuous with 5 nm resolution); (b) telescopic reflectance spectra of 10–20 km (diameter) areas on the lunar surface (.3 to 1.1 μm, 30 nm resolution); (c) telescopic spectral imagery (spatial resolution 1–50 km; 2 to 4 band passes between .38 and 1.0 μm); and (d) telescopic infrared reflectance spectra of 20 km areas (.65 to 2.1 μm, continuous with 10–20 nm resolution). Because of the differences in spatial and spectral resolution, spectral coverage, and precision, it is often difficult for anyone not intimately familiar with reflectance measurements to make consistent and coherent use of the data available.

The purpose of this study is to distill the currently available reflectance data for the lunar maria into one map and to discuss the compositional information such a map contains. The discussion centers around the spectral properties of mature lunar soils and is similar to that found in Pieters (1977a). Spectra for rocks, breccias and craters contain more well-defined absorption bands than soils, but a program to obtain such telescopic spectra of fresh (immature) surfaces has only begun. In this study a few comparisons of spectral data with orbital chemical measurements are also made, but a complete synthesis of the spectral data with other remote sensing data is beyond the scope of this discussion.

Although ~80% of the spectral data is in digital form, the map that is presented here is not computer-generated and thus relies on subjective judgment. However,

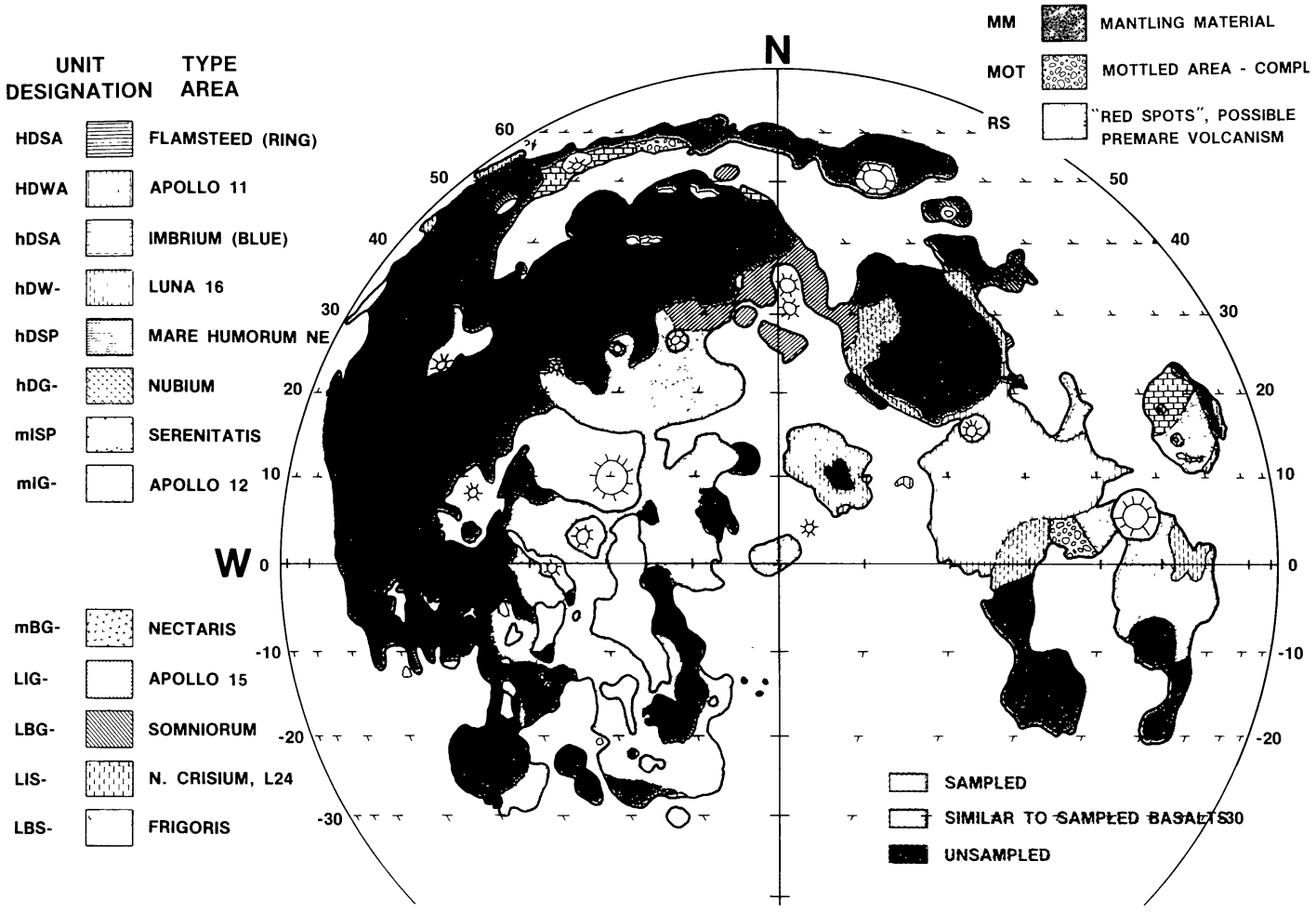

Plate 1. Sampled and unsampled basalt types on the frontside of the moon. The base map shows the distribution of distinct mare basalt units as derived from all available spectral reflectance data and multispectral imagery (see Pieters, these *Proceedings*). The unit designation represents values for four measurable parameters (UV/VIS ratio, albedo, strength of the 1 μm band, and strength of a 2 μm band). Since each of these parameters is dependent on composition of the surface, basalt units which are distinctly different from the sampled units can be identified and mapped on the basis of spectral properties. About two-thirds of the nearside mare surface, which includes up to eight distinct major basalt types, remains unsampled.

1978LPSC....9.2825P

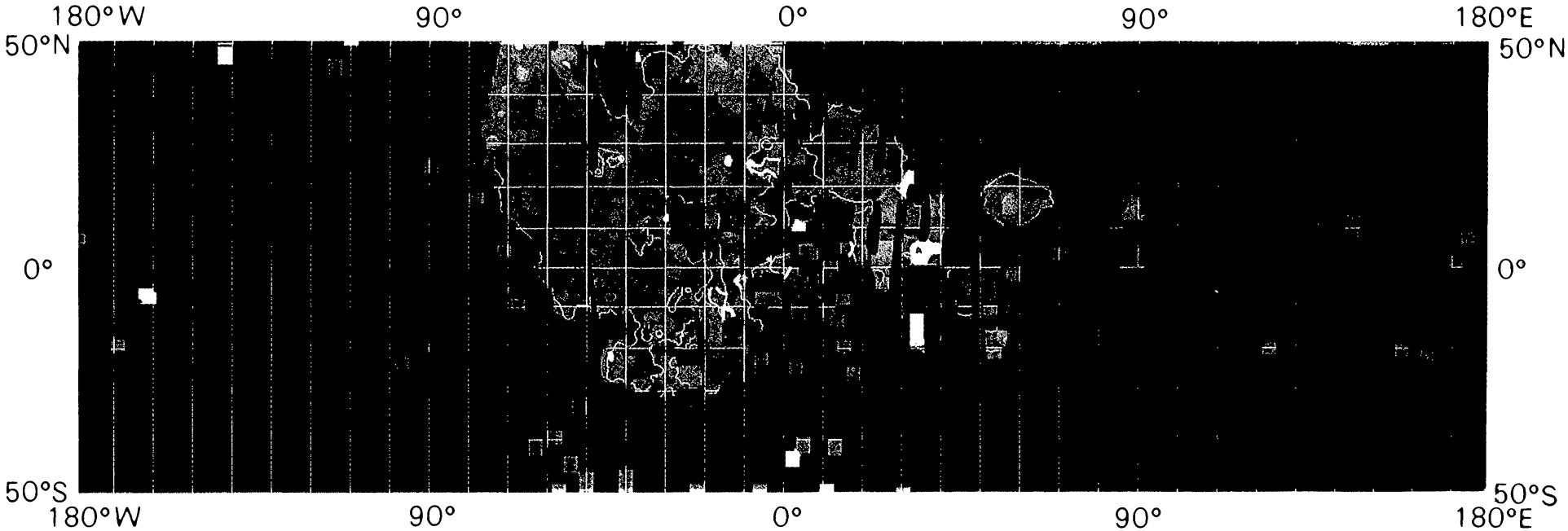

Plate 2. Relative ages of the maria and light plains. This map is the final product of a mapping effort that involved using both crater density and crater morphology techniques. The new data for Mare Crisium, Marginis, and Smythii are based on crater density, all others are based on crater morphology. The two data sets have been correlated using the relationship of crater density to D_L. The absolute age of each unit has been estimated based on radiometric ages of Apollo samples for absolute calibration. The ages are: 2.5 ± 0.5 b.y. (violet); 3.2 ± 0.2 b.y. (blue); 3.5 ± 0.1 b.y. (cyan); 3.65 ± 0.05 b.y. (green); 3.75 ± 0.05 b.y. (yellow); 3.85 ± 0.05 b.y. (red); to 3.90 ± 0.5 b.y. (white). (See Boyce, J. M. and Johnson, D., these *Proceedings*.)

1978LPSC....9.2825P

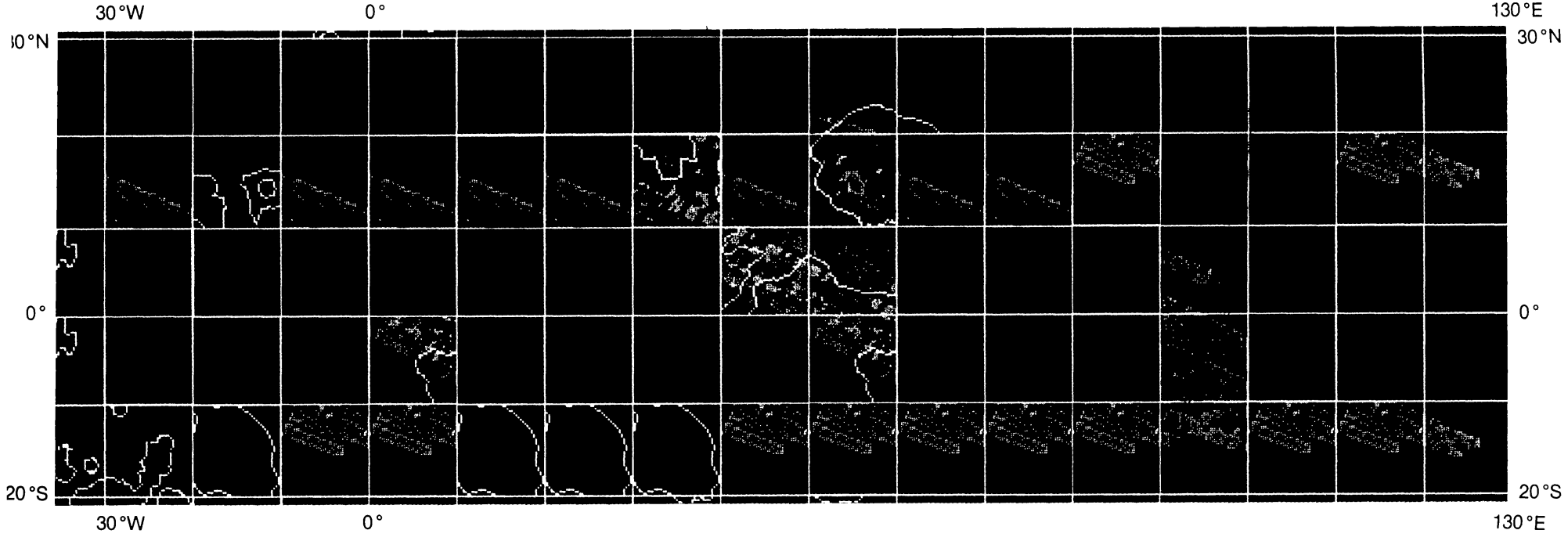

Plate 3. Variations in the **Mg/Si** ratio of the lunar surface are shown by the Apollo 15 orbital X-ray fluorescence data. **Mg/Si** intensity ratios are mapped using a color scheme ranging froom violet (0.3–0.5), dark blue (0.5–0.7), light blue (0.7–0.9), to red (>0.9). Maria outlined here are Serenitatis, Imbrium, Tranquillitatis, Crisium, and Fecunditatis. The prominent red spot at about longitude 87° is in Mare Smythii. The red dot in Crisium (~55° long.) is Picard Crater. Red dots east of Serenitatis are in the vicinity of the Apollo 17 landing site, and the long red area in southwestern Serenitatis is associated with the Sulpicius Gallus area. Many features seen in these improved **Mg/Si** data are discussed in Hubbard *et al.* (1978a) and in Hubbard and Keith (1978). Two minor defects exist in this image because the solar behavior during two orbits (57 and 67) was significantly different from that for which the empirical solar correction procedure was calibrated. In both cases, this resulted in a band of values erroneously low by one color step. The effect of orbit 67 (located at the lower edge of the data covering Tranquillitatis and Fecunditatis) is weakened by being averaged with adjacent data. Much of orbit 57 lacks data, so it has contributed only the dark blue streak in Fecunditatis from about 52° long., 7° lat. to 61° long., −2° lat. The band of data above the main body of data is for three orbits of data taken before orbit circularization. They were collected at lower altitudes and have higher spatial resolution; here they are treated as having normal resolution. The data were smoothed using a sliding nested box filter imitating the angular response of the X-ray detectors. The dimensions of the boxes and corresponding weights are: 0.75° × 0.75°, 0.417; 1.25° × 1.25°, 0.294; 1.75° × 1.75°, 0.206; and 2.75° × 2.75°, 0.083. Data from greater than 50° phase angle were rejected. This plate was prepared by Faith Vilas, Eric Eliason, Norman Hubbard, and James Keith. These data were reduced at the Johnson Space Center using data obtained from the National Space Science Data Center. Undesirable solar effects were removed by a procedure developed at JSC (see Hubbard *et al.*, 1978a, b, c). The conversion to image format was done at the USGS Image Processing Facility, Flagstaff, by Eric Eliason.

References

Hubbard N. J. and Keith J. E. (1978) A declaration of independence for Mg/Si. *Proc. Lunar and Planet. Sci. Conf. 9th.* This volume.

Hubbard N. J., Vilas F. and Keith J. E. (1978a) From Serenity to Langemak: A regional chemical setting for Mare Crisium. In *Mare Crisium: The View from Luna 24* (R. B. Merrill and J. J. Papike, eds.), p. 000–000. Pergamon, New York.

Hubbard N. J., Vilas F. and Keith J. E. (1978b) Ot Yasnosti do Langemaka: Regionalnoye polozheniye dlya Morya Krizisov. In *Luna-24*: sbornik statye. V. pechati (in Russian). In press.

Hubbard N. J., Vilas F. and Keith J. E. (1978c) Solar corrections for the Apollo orbital X-ray fluorescence data (abstract). In *Lunar and Planetary Science IX*, p. 558–560. Lunar and Planetary Institute, Houston.

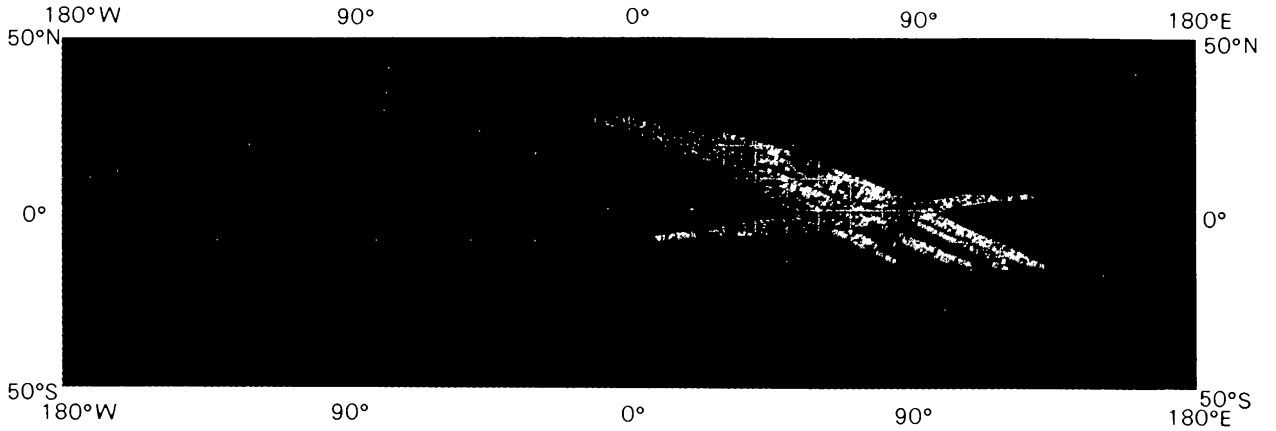

Plate 4. X-ray fluorescence **Al/Si** intensity ratios. This map shows substantial improvement over previous renditions because it has been corrected for variation in solar activity by the use of independent solar flux measurements made by the SOLRAD spacecraft in earth orbit. Colors correspond to **Al/Si** intensity ratios as follows: Red, 1.91 to 1.31; Yellow, 1.30 to 1.14; Green, 1.13 to 1.00; Cyan, .990 to .840; Blue, .830 to .700; Violet, .690 to .365. (See Clark, P. E., and Adler, I., these *Proceedings*.)

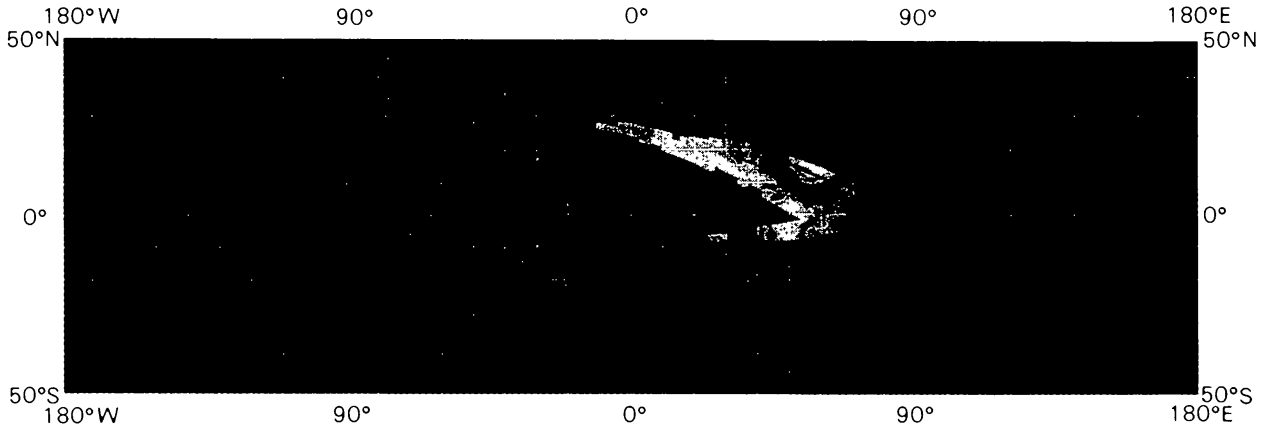

Plate 5. Color correlation to **Al/Si** intensity ratios and normal albedo, (see frontispiece (1977) *Proc. Lunar Sci. Conf. 8th*). Normal albedo ranges from .095 to .172; **Al/Si** ratios range from .365 to 1.91. Colors correspond to ranges of data as follows: Pink, **Al/Si** .365 to .950; Albedo .095 to .103; Lavender, **Al/Si** .365 to .095; Albedo .104 to .123; Blue, **Al/Si** .365 to .950; Albedo .124 to .172; Light Orange, **Al/Si** .960 to 1.15; Albedo .104 to .123; Purple, **Al/Si** .960 to 1.15; Albedo .124 to .172; Yellow, **Al/Si** 1.16 to 1.90; Albedo .095 to .103; Dark Orange, **Al/Si** 1.16 to 1.91; Albedo .104 to .123; Maroon, **Al/Si** 1.16 to 1.91; Albedo .124 to .172. Predominance of red shades indicates a positive linear correlation. (See Clark, P. E., Eliason, E., Andre, C. G., and Adler, I., these *Proceedings*).

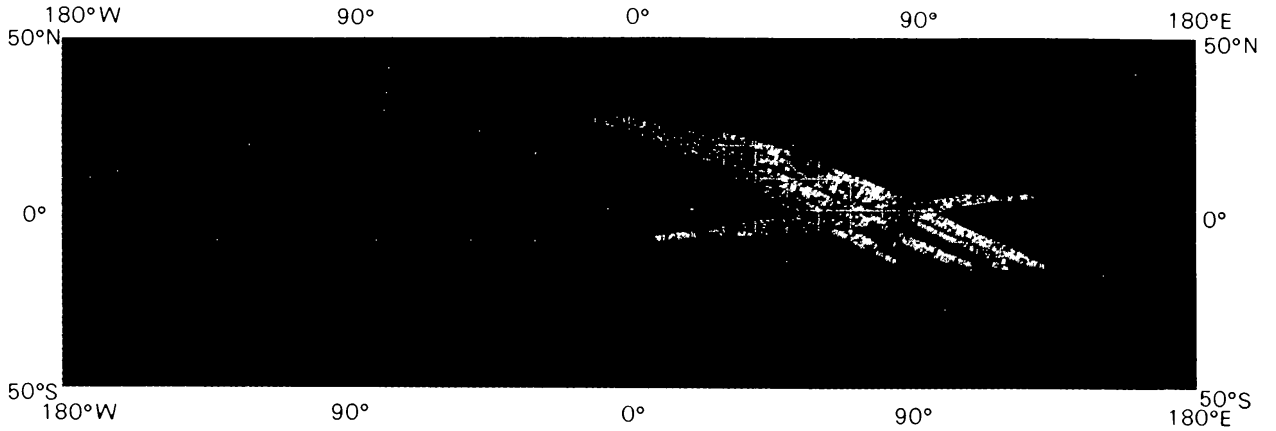

Plate 4. X-ray fluorescence **Al/Si** intensity ratios. This map shows substantial improvement over previous renditions because it has been corrected for variation in solar activity by the use of independent solar flux measurements made by the SOLRAD spacecraft in earth orbit. Colors correspond to **Al/Si** intensity ratios as follows: Red, 1.91 to 1.31; Yellow, 1.30 to 1.14; Green, 1.13 to 1.00; Cyan, .990 to .840; Blue, .830 to .700; Violet, .690 to .365. (See Clark, P. E., and Adler, I., these *Proceedings*.)

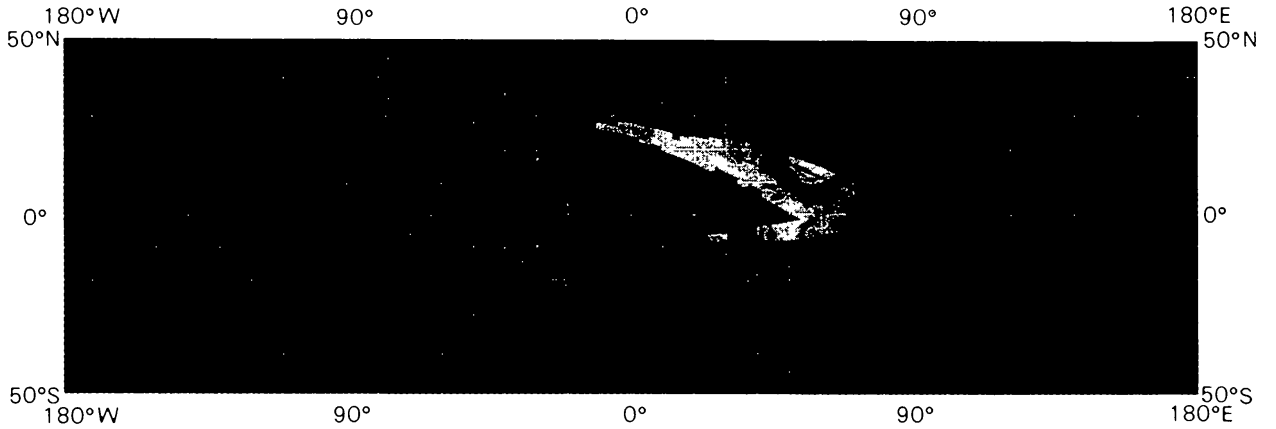

Plate 5. Color correlation to **Al/Si** intensity ratios and normal albedo, (see frontispiece (1977) *Proc. Lunar Sci. Conf. 8th*). Normal albedo ranges from .095 to .172; **Al/Si** ratios range from .365 to 1.91. Colors correspond to ranges of data as follows: Pink, **Al/Si** .365 to .950; Albedo .095 to .103; Lavender, **Al/Si** .365 to .095; Albedo .104 to .123; Blue, **Al/Si** .365 to .950; Albedo .124 to .172; Light Orange, **Al/Si** .960 to 1.15; Albedo .104 to .123; Purple, **Al/Si** .960 to 1.15; Albedo .124 to .172; Yellow, **Al/Si** 1.16 to 1.90; Albedo .095 to .103; Dark Orange, **Al/Si** 1.16 to 1.91; Albedo .104 to .123; Maroon, **Al/Si** 1.16 to 1.91; Albedo .124 to .172. Predominance of red shades indicates a positive linear correlation. (See Clark, P. E., Eliason, E., Andre, C. G., and Adler, I., these *Proceedings*).

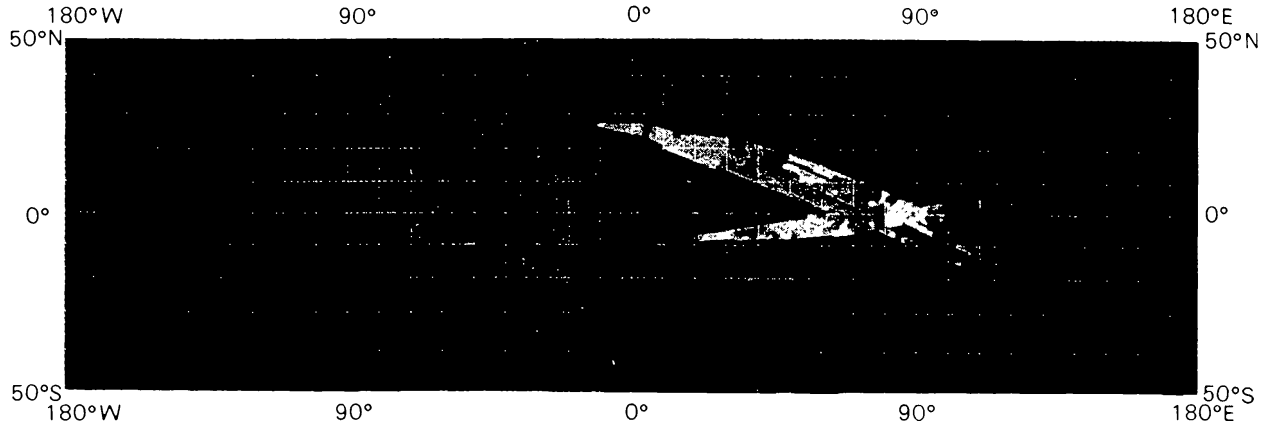

Plate 6. Color correlation of **Al/Si** ratios and laser altimetry data (see frontispiece (1977) *Proc. Lunar Sci. Conf. 8th*). Elevations range from 1733 km to 1741 km above the moon's center-of-mass; **Al/Si** ratios range from .365 to 1.91. Colors correspond to ranges of data as follows: Pink, **Al/Si** .365 to .950, elevation 1733 to 1735. 2; Lavender, **Al/Si** .365 to .950, elevation 1735.3 to 1736.6; Blue, **Al/Si** .365 to .950, elevation 1736.7 to 1741; Light Orange, **Al/Si** .960 to 1.15, elevation 1733 to 1735.2; Red, **Al/Si** .960 to 1.15, elevation 1735.3 to 1736.6; Purple, **Al/Si** .960 to 1.15, elevation 1736.7 to 1741; Yellow, **Al/Si** 1.16 to 1.91, elevation 1733 to 1735.2; Dark Orange, **Al/Si** 1.16 to 1.91, elevation 1735.3 to 1736.6; Maroon, **Al/Si** 1.16 to 1.91, elevation 1736.7 to 1741. Predominance of red shades indicates a positive linear correlation. (See Clark, P. E., Eliason, E., Andre, C. G., and Adler, I., these *Proceedings*.)

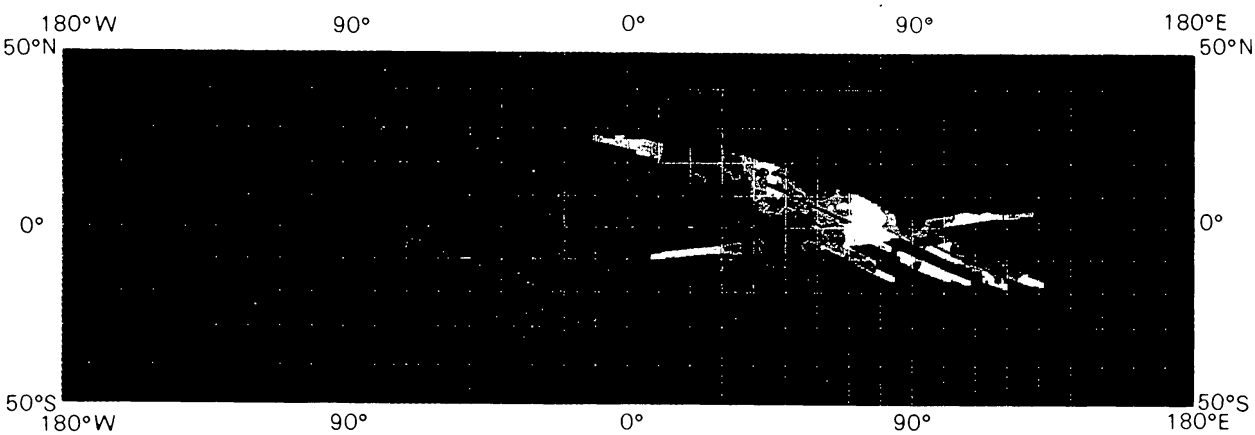

Plate 7. Color correlation of **Al/Si** ratios and gamma ray data (see frontispiece, 1977, *Proc. Lunar Sci. Conf. 8th*) in the 2.75 to 8.60 MEV range (Fe). Fe data range from 19.4 to 21.2 counts/seconds; Al/Si ratios range from .365 to 1.91. Color corresponds to ranges of data as follows: Pink, **Al/Si** .365 to .950, Fe 19.4 to 20.1; Lavender, **Al/Si** .365 to .950, Fe 20.2 to 20.5; Blue, **Al/Si** .365 to .950, Fe 20.6 to 21.2; Light Orange, **Al/Si** .960 to 1.15, Fe 19.4 to 20.1; Red, **Al/Si** .960 to 1.15, Fe 20.2 to 20.5; Purple, **Al/Si** .960 to 1.15, Fe 20.6 to 21.2; Yellow, **Al/Si** 1.16 to 1.91, Fe 19.4 to 20.1; Dark Orange, **Al/Si** 1.16 to 1.91, Fe 20.2 to 20.5; Maroon, **Al/Si** 1.16 to 1.91, Fe 20.6 to 21.2. Predominant primary colors blue, red, and yellow indicate an inverse linear correlation. (See Clark, P. E., Eliason, E., Andre, C. G., and Adler, I., these *Proceedings*.)

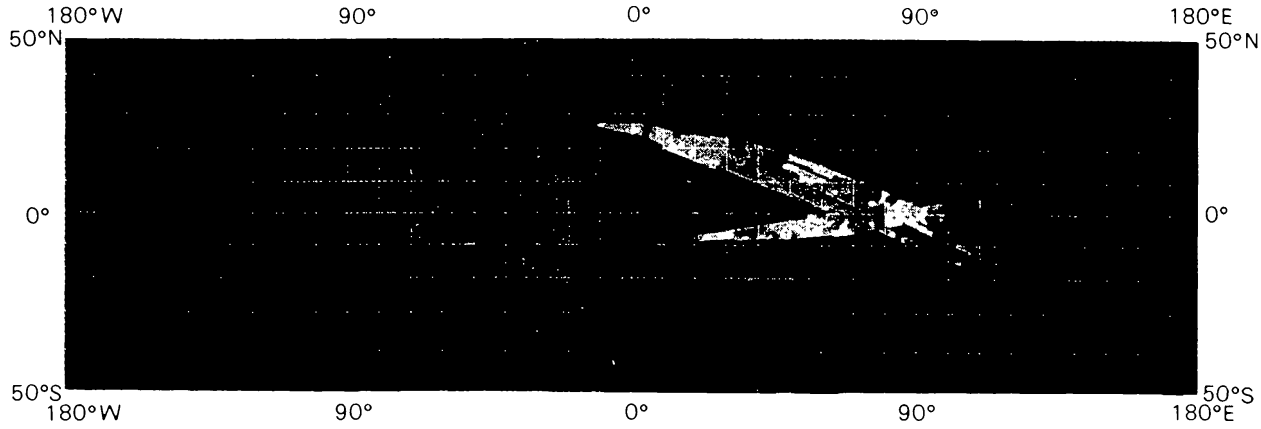

Plate 6. Color correlation of **Al/Si** ratios and laser altimetry data (see frontispiece (1977) *Proc. Lunar Sci. Conf. 8th*). Elevations range from 1733 km to 1741 km above the moon's center-of-mass; **Al/Si** ratios range from .365 to 1.91. Colors correspond to ranges of data as follows: Pink, **Al/Si** .365 to .950, elevation 1733 to 1735. 2; Lavender, **Al/Si** .365 to .950, elevation 1735.3 to 1736.6; Blue, **Al/Si** .365 to .950, elevation 1736.7 to 1741; Light Orange, **Al/Si** .960 to 1.15, elevation 1733 to 1735.2; Red, **Al/Si** .960 to 1.15, elevation 1735.3 to 1736.6; Purple, **Al/Si** .960 to 1.15, elevation 1736.7 to 1741; Yellow, **Al/Si** 1.16 to 1.91, elevation 1733 to 1735.2; Dark Orange, **Al/Si** 1.16 to 1.91, elevation 1735.3 to 1736.6; Maroon, **Al/Si** 1.16 to 1.91, elevation 1736.7 to 1741. Predominance of red shades indicates a positive linear correlation. (See Clark, P. E., Eliason, E., Andre, C. G., and Adler, I., these *Proceedings*.)

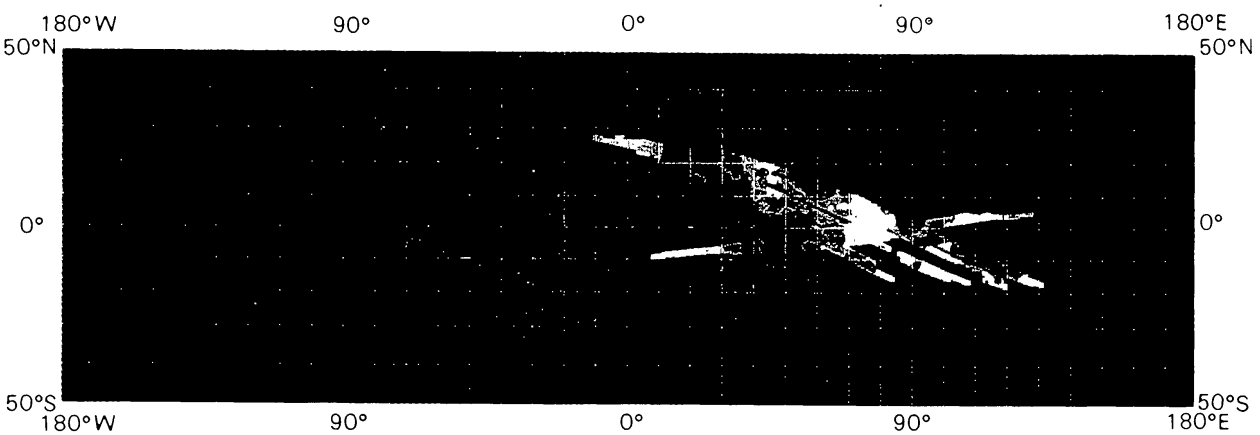

Plate 7. Color correlation of **Al/Si** ratios and gamma ray data (see frontispiece, 1977, *Proc. Lunar Sci. Conf. 8th*) in the 2.75 to 8.60 MEV range (Fe). Fe data range from 19.4 to 21.2 counts/seconds; Al/Si ratios range from .365 to 1.91. Color corresponds to ranges of data as follows: Pink, **Al/Si** .365 to .950, Fe 19.4 to 20.1; Lavender, **Al/Si** .365 to .950, Fe 20.2 to 20.5; Blue, **Al/Si** .365 to .950, Fe 20.6 to 21.2; Light Orange, **Al/Si** .960 to 1.15, Fe 19.4 to 20.1; Red, **Al/Si** .960 to 1.15, Fe 20.2 to 20.5; Purple, **Al/Si** .960 to 1.15, Fe 20.6 to 21.2; Yellow, **Al/Si** 1.16 to 1.91, Fe 19.4 to 20.1; Dark Orange, **Al/Si** 1.16 to 1.91, Fe 20.2 to 20.5; Maroon, **Al/Si** 1.16 to 1.91, Fe 20.6 to 21.2. Predominant primary colors blue, red, and yellow indicate an inverse linear correlation. (See Clark, P. E., Eliason, E., Andre, C. G., and Adler, I., these *Proceedings*.)

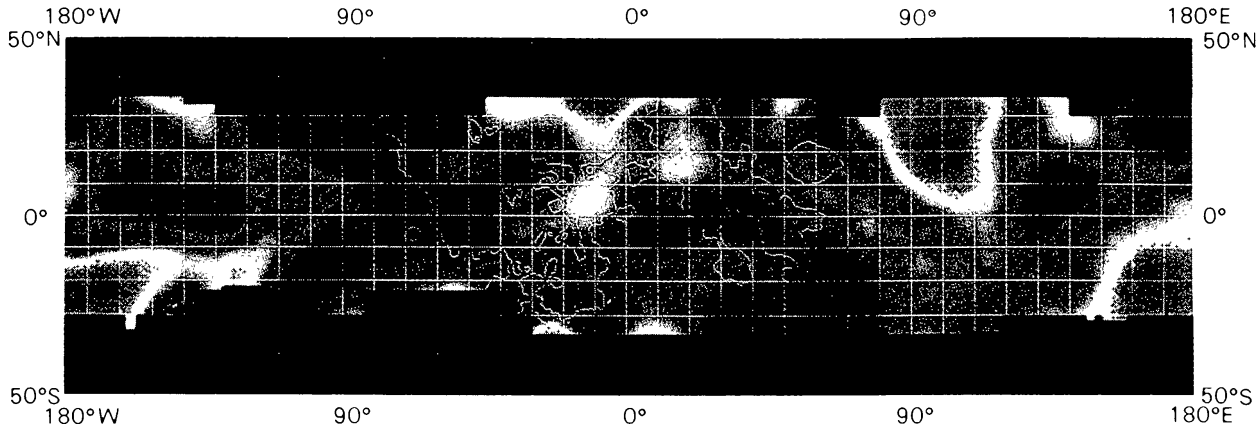

Plate 8. Magnitude of the inward component of the lunar surface remanent magnetic field derived from high energy (14 keV) electron reflection measurements by detectors aboard the Apollo 15 and 16 subsatellites. This low resolution image was averaged over 15° cells for comparison with the Explorer 35 map in Plate 9. The colors represent magnetic field magnitude values ranging from less than 0.2 gamma (purple) to greater than 5.0 gammas (red). (See Lichtenstein, B. R., Coleman, P. J., and Russell, C. T., these *Proceedings.*)

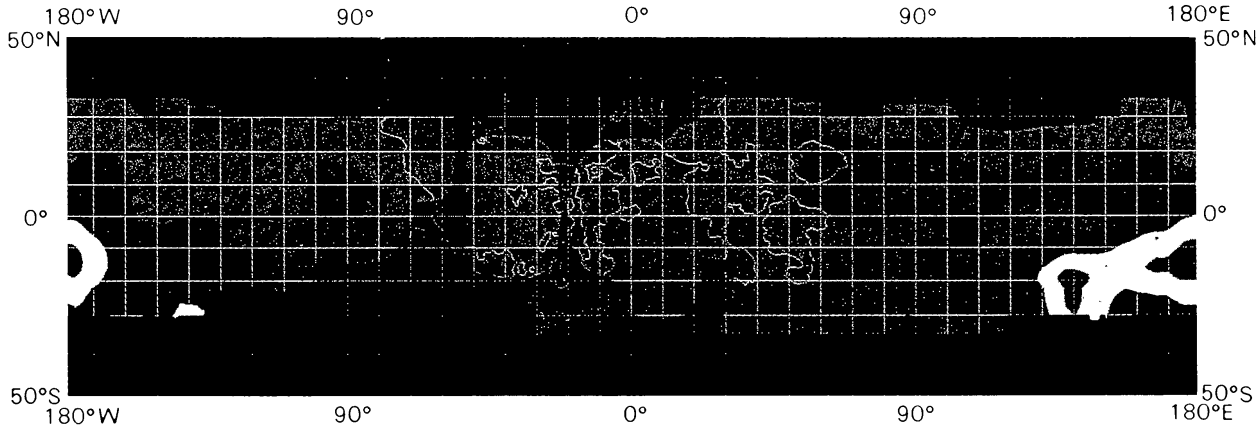

Plate 9. Map from Explorer 35 data of the occurrence rate of interplanetary magnetic field magnitude disturbances associated with selenographic regions at the lunar limbs. The colors represent occurrence rates ranging from zero (dark blue) to greater than 0.45 (red). (See Lichtenstein, B. R., Coleman, P. J., and Russell, C. T., these *Proceedings.*)

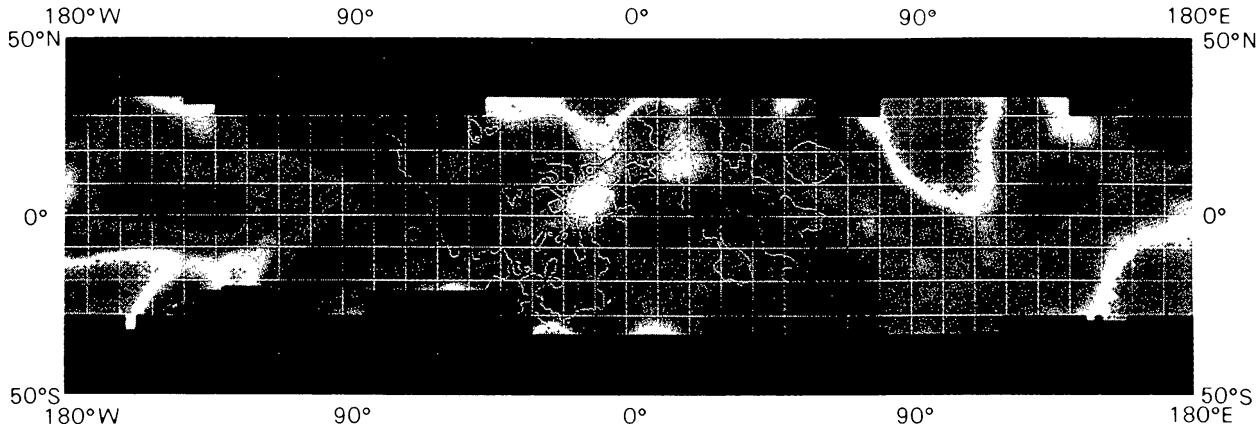

Plate 8. Magnitude of the inward component of the lunar surface remanent magnetic field derived from high energy (14 keV) electron reflection measurements by detectors aboard the Apollo 15 and 16 subsatellites. This low resolution image was averaged over 15° cells for comparison with the Explorer 35 map in Plate 9. The colors represent magnetic field magnitude values ranging from less than 0.2 gamma (purple) to greater than 5.0 gammas (red). (See Lichtenstein, B. R., Coleman, P. J., and Russell, C. T., these *Proceedings.*)

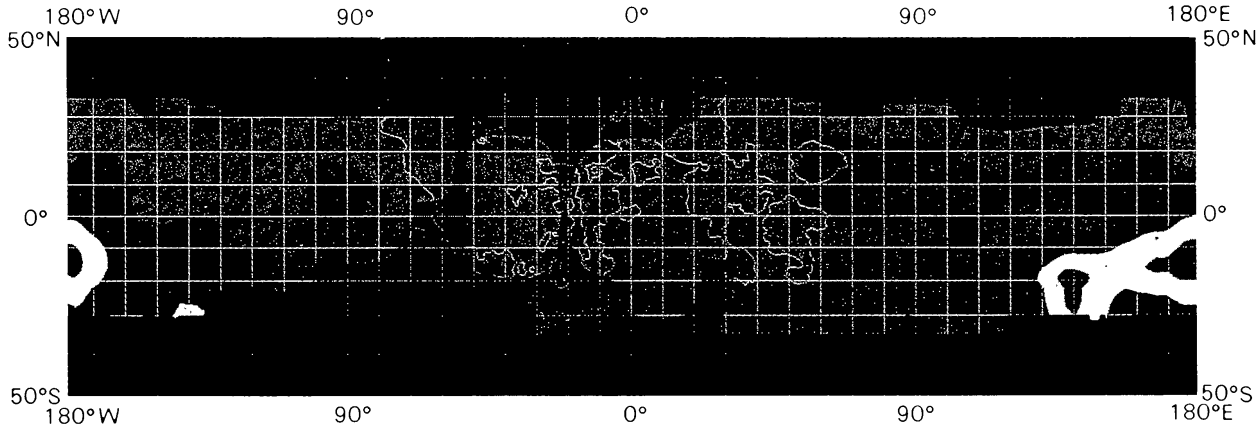

Plate 9. Map from Explorer 35 data of the occurrence rate of interplanetary magnetic field magnitude disturbances associated with selenographic regions at the lunar limbs. The colors represent occurrence rates ranging from zero (dark blue) to greater than 0.45 (red). (See Lichtenstein, B. R., Coleman, P. J., and Russell, C. T., these *Proceedings.*)

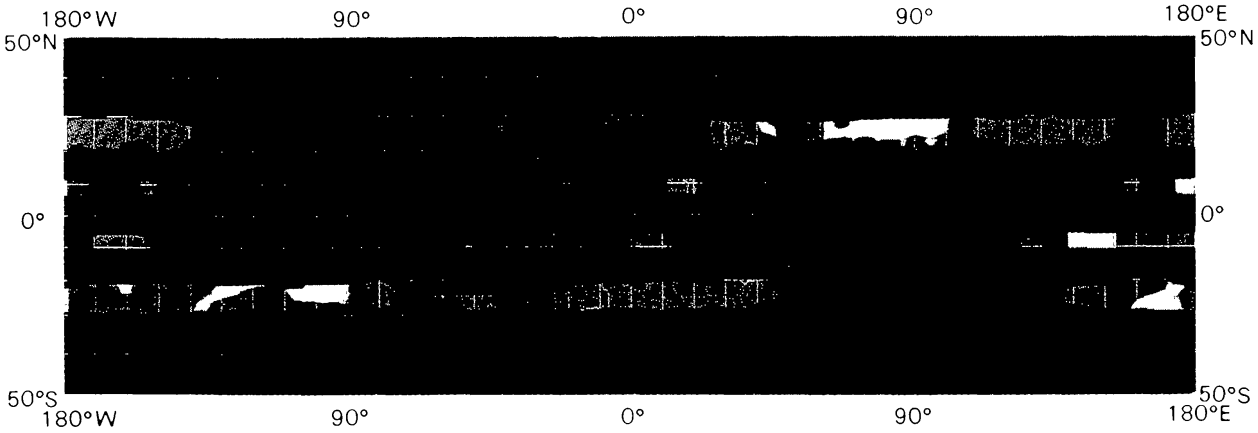

Plate 10. Map of the occurrence rate of magnetic disturbances associated with selenographic regions at the lunar limb derived from Apollo 15 and 16 subsatellite magnetometer measurements. The colors represent occurrence rates ranging from zero (dark blue) to greater than 0.8 (red). (See Lichtenstein, B. R., Coleman, P. J., and Russell, C. T., these *Proceedings.*)

using this method of data compilation, most (if not all) extraneous or confusing effects (such as registration problems in spectral ratio images) can be identified and excluded leaving the results much "cleaner." It should be kept in mind that more information exists in the data than can be represented in a single map. What has been distilled for presentation here is the extent of the major distinct basalt types on the lunar nearside. Much more spectral information exists for fine details of mapping and characterizing various regions.

The part of the electromagnetic spectrum utilized for remote sensing reflectance information has been from .3 μm to 2.5 μm (e.g., see Head *et al.*, 1978a). The short wavelength limit of telescopic reflectance measurements is determined by atmospheric O_3 absorptions that leave the atmosphere effectively opaque shortwards of .3 μm. Although the infrared measurements are also affected by atmospheric absorptions (primarily H_2O), the thermal component of radiation, which becomes increasingly significant beyond 2.5 μm for the moon, limits reflectance studies to wavelengths shorter than 2.5 μm.

The spectral character of light reflected from a mare surface with a well-developed soil is nearly the same for any lunar area: the spectrum is almost monotonically red (increasing reflectance toward longer wavelengths) with small absorption features near 1 μm and sometimes 2 μm that can be seen in Fig. 1 and 2. Small variations of this spectrum occur between maria on the moon due to differences in chemical composition of the soil and include: (1) variations in continuum slope largely in the ultraviolet (UV) and visible (VIS) (differences up to about 10%); (2) variations in overall albedo (A = 7.5% to 12%); and (3) differences in the nature of the 1 μm and 2 μm bands (depth, center wavelength, width, symmetry). To discern the small spectral differences, each mare region is usually compared to a standard area in central Serenitatis (MS2, or d on Fig. 1). Relative reflectance spectra shown in Fig. 3 are such comparative spectra in which each mare spectrum has been divided by the spectrum for MS2. These relative reflectance spectra were chosen from the classification of Pieters and McCord (1976) to demonstrate the range of variability in the spectra for mare soils.

Four measurable parameters were chosen which would maximize the probability of distinguishing general mineralogical and chemical differences between mature soils developed on basalt units: (1) UV/VIS slope; (2) albedo; (3) depth of the 1 μm band; and (4) depth of the 2 μm band. The data sources for each parameter are mentioned in the first section. The unit map is presented and effects of composition on each parameter are examined in subsequent sections. Interpretations of the data for a few unsampled basalt types are discussed.

II. DATA SOURCES

A. UV/VIS ratio

The lunar continuum is generally smooth between .3 and .7 μm with increasing reflectance toward longer wavelengths (Fig. 1). A slight inflection sometimes occurs near .4 μm. The absolute slope of this continuum varies considerably during

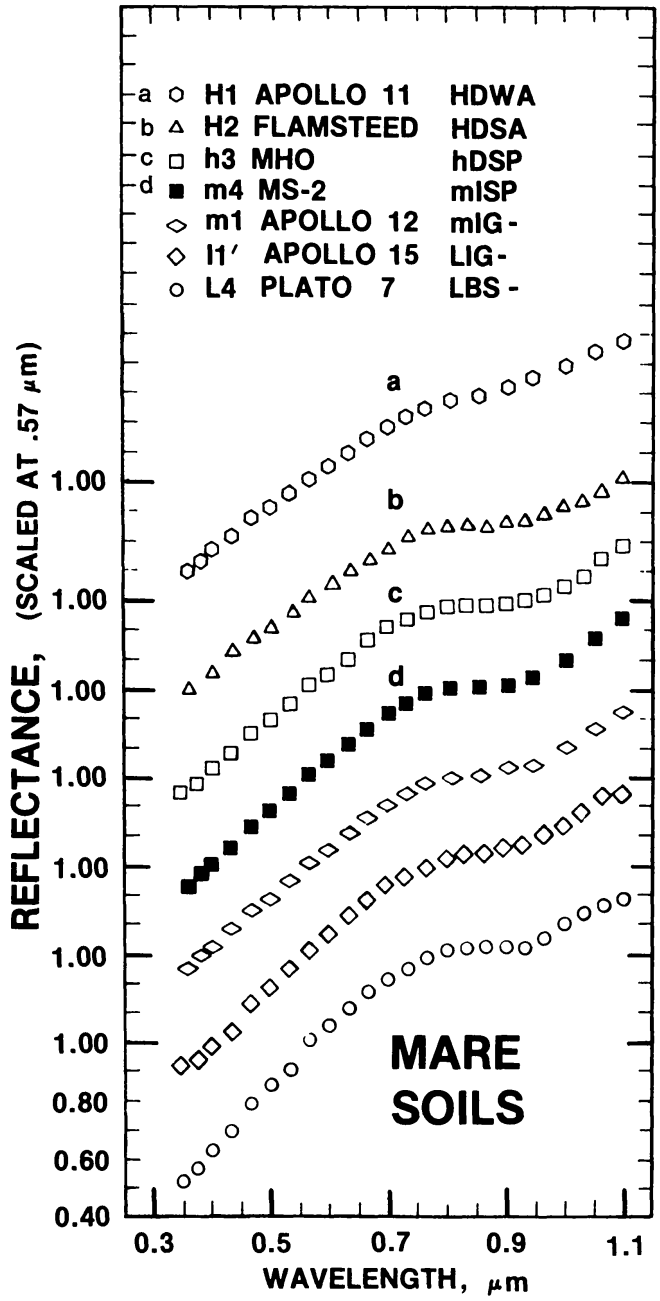

Fig. 1. Telescopic reflectance spectra of representative mare soils from .3 to 1.1 μm. All spectra are scaled to unity at .57 μm. Spectrum *d* is for the telescopic standard area MS2 in central Serenitatis. The letter and number designation to the left of each spot name refers to the classification of Pieters and McCord (1976). The four-letter designation to the right of the spot name is the more complete unit designation discussed in this paper.

a single lunation: the moon becomes redder with increasing phase angle. However, the relative spectral differences, or differences between two different regions, remain roughly the same, regardless of viewing geometry, between about 10° and 50° phase angle (McCord, 1969). The relative slope of a mare continuum can vary

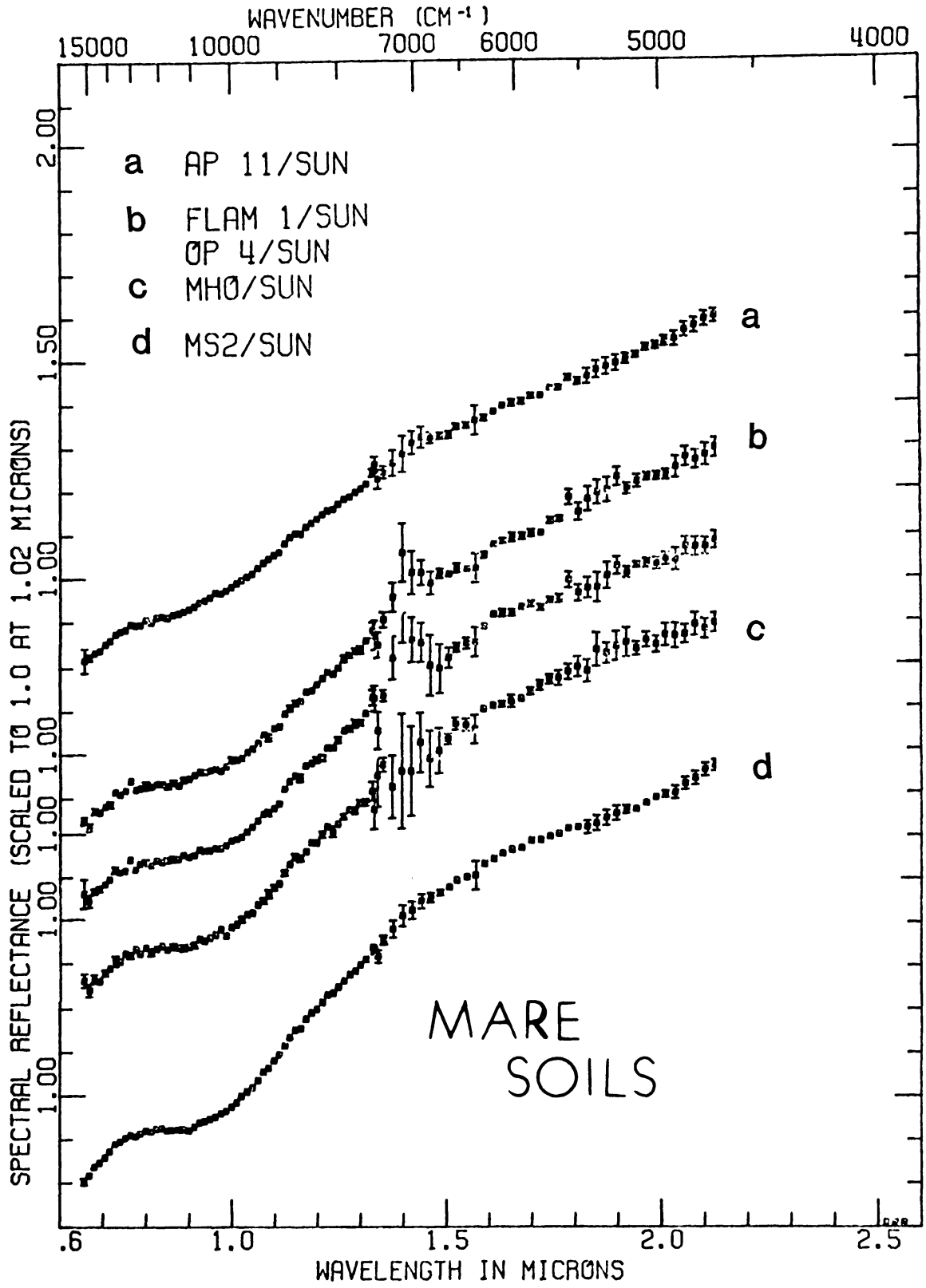

Fig. 2. Telescopic reflectance spectra of five mare regions from .65 to 2.1 μm. All spectra are scaled to unity at 1.0 μm.

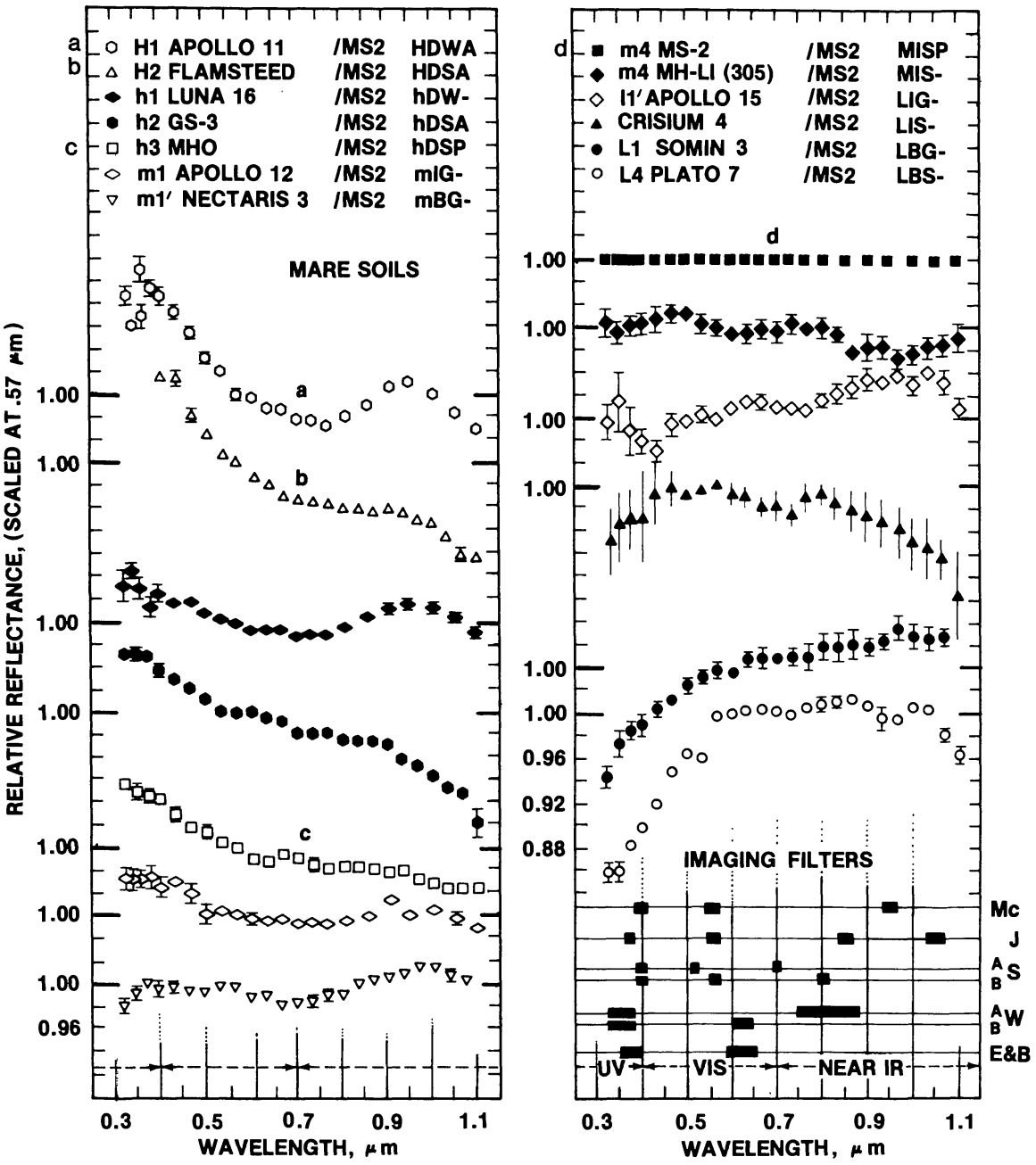

Fig. 3. Relative telescopic reflectance spectra .3 to 1.1 μm of representative mare soils. All spectra are relative to MS2 and scaled to unity at .57 μm. The letter and number designation to the left of each spot name refer to the classification of Pieters and McCord (1976). The four-letter designation to the right of the spot name is the more complete unit designation discussed in this paper. The bandpasses for various forms of multi-spectral images are indicated in the lower right. Mc = McCord *et al.* 1976, 1978; J = Johnson *et al.* 1977, 1978; S = Soderblom (A) 1970, (B) Frontispiece, 1977; W = Whitaker (A) 1972, (B) pers. comm., 1976; E&B = Evsyukov and Barabashov, 1973.

up to about 10% from the average (McCord, 1968). The difference in continuum slope between two different regions is usually measured as a relative spectral ratio derived from measurements of both areas with two different filters—one filter centered in the ultraviolet (UV) spectral region and the other in the visible (VIS). A relative UV/VIS ratio R for area A relative to area S thus has the form:

$$R = \frac{A_{(UV)}}{A_{(VIS)}} \div \frac{S_{(UV)}}{S_{(VIS)}}.$$

where $A_{(\lambda)}$ is the value of reflected radiation at region A for the spectral region λ and $S_{(\lambda)}$ is the value of reflected radiation at a standard area (e.g., MS2) for the spectral region λ. An advantage of relative spectral ratios over an absolute spectral measurement is that atmospheric and instrumental effects cancel in the simple ratio. For mare soils the relative differences in UV/VIS spectral ratio have been measured both from spectrophotometry of individual areas (e.g., Fig. 3) and from spectral imagery for large regions.

Three forms of multispectral imagery of the lunar nearside were used in this study: (1) digital vidicon (McCord *et al.*, 1976; 1978; Johnson *et al.*, 1977; 1978, pers. comm.); (2) line scan (Soberblom, 1970; Frontispiece, 1977); and (3) color difference photography (Whitaker, 1972; 1976; Evsyukov and Barabashov, 1973a) (see Head *et al.*, 1978a for discussion of techniques). The vidicon and line scan techniques produce digital images with a precision of about 1%. The photographic technique is most useful in analogue form; when digitized, the precision is estimated to be 2–3%. The imaging bandpasses used by various groups are shown in the bottom right of Fig. 3. It can be seen that all groups have some possible form of UV/VIS ratio, although the wavelength of the two bands, and thus the relative ratio, is not the same for each measurement. Using the numerical information provided by the spectra for individual small areas such as seen in Fig. 3, these various forms of UV/VIS images have been roughly calibrated to each other and checked for consistency. The major sources for ~150 relative reflectance spectra of mature mare regions are McCord (1968) and Pieters and McCord (1976). A few unpublished mare spectra also exist. Some remote sensing studies of particular regions include additional spectra: Mare Humorum (Johnson *et al.*, 1973; Pieters *et al.*, 1975), Mare Crisium (Head *et al.*, 1978b) and the Flamsteed region of Oceanus Procellarum.

B. Albedo

The albedo of a surface is a measure of its overall brightness. Particular uses of the word "albedo" (e.g., bond, geometric, normal) refer to specific ways the brightness is derived. "Normal" albedo is the most commonly measured and refers to the % reflectance at zero degrees phase angle, or full moon. (In reality the measurements are obtained at 2–5° phase angle and extrapolated to 0°). Three published maps of the normal albedo of the moon were used in this study: Pohn and Wildey (1970); Evsyukov and Barabashov (1973b) and (1973c). The nominal spatial resolution of these maps is from 3 to 6 km. The first two maps, which are

generally similar in detail to each other, were obtained using the astronomical "visible" filter centered near .55 μm with a broad band pass of about 800 nm. The third map was obtained using a filter centered at .62 μm and shows a somewhat different distribution of very dark maria. These quantitative maps were used to identify major regional differences in albedo for the mare surfaces. Earthbased photographs were used to estimate the relative albedo for units that require higher spatial resolution and for units that contained a significant number of rays such that the low resolution normal albedo maps were not necessarily valid for the general mare surface.

C. 1 μm band

The absorption band near 1 μm (Figs. 1 and 2) varies in both strength and general nature (wavelength, symmetry, etc.). For rocks this absorption feature (and the one at 2 μm) is strong, but for lunar soils the 1 μm band is a subtle feature superimposed on the steeply sloped continuum. As can be seen from the representative relative spectra of soils in Fig. 3, there is no simple combination of spectral bands that can describe the variations in the 1 μm feature. The general spectral types discerned from such spectra have been classified (Pieters and McCord, 1976), but description of the full nature of the 1 μm band requires data into the infrared (IR). There are two important reasons why IR data well beyond 1.1 μm are necessary to examine the nature of the 1μm feature. First, the effects of overall slope of a lunar continuum must be eliminated from the superimposed absorption features. In order to estimate a lunar continuum, data are required on both sides of the 1 μm feature. Second, the wings of the 1 μm band often extend to 1.4 μm depending on the combination of minerals present. The structure of the spectral feature varies greatly between .9 μm and 1.3 μm as a function of mineralogy.

In Fig. 4 continua have been fit through .73 μm and 1.5 μm for IR spectra *a* and *d* of Fig. 2. Plotted in energy units above the spectra are the residual absorption features. The 5 residual spectra (continuum removed) of Fig. 5 show some of the variations in character of the 1 μm bands for these mare soils: depth varies by a factor of 2, width varies by about 12%, and the wavelength of the overall band center ranges from 1.00 μm to 1.07 μm. The asymmetry of the 1 μm feature indicates it is a composite band of at least two components.

Since such complete IR spectra do not exist for most mare surfaces, a band parameter was chosen for this study that could be at least estimated from the .3 to 1.1 μm spectra, namely the strength of the 1 μm absorption feature. In Figs. 2 and 5 spectrum *a* has a relatively weak 1 μm band whereas spectra *b*, *c*, and *d* have strong 1 μm bands. A weak band translates into a bump in the relative spectrum *a* for Apollo 11 in Fig. 3, whereas a strong band is indicated by a generally lower relative reflectance ratio in the 1 μm region (e.g., spectra *b*, *c*, *d*). The strength of the 1 μm band was estimated using the spectra in the classification scheme of Pieters and McCord (1976) as well as a few unpublished spectra. When no spectra exist for a given unit the strength of the 1 μm feature was estimated from the near IR vidicon images of McCord *et al.* (1976, 1978) and Johnson *et al.* (1977, 1978).

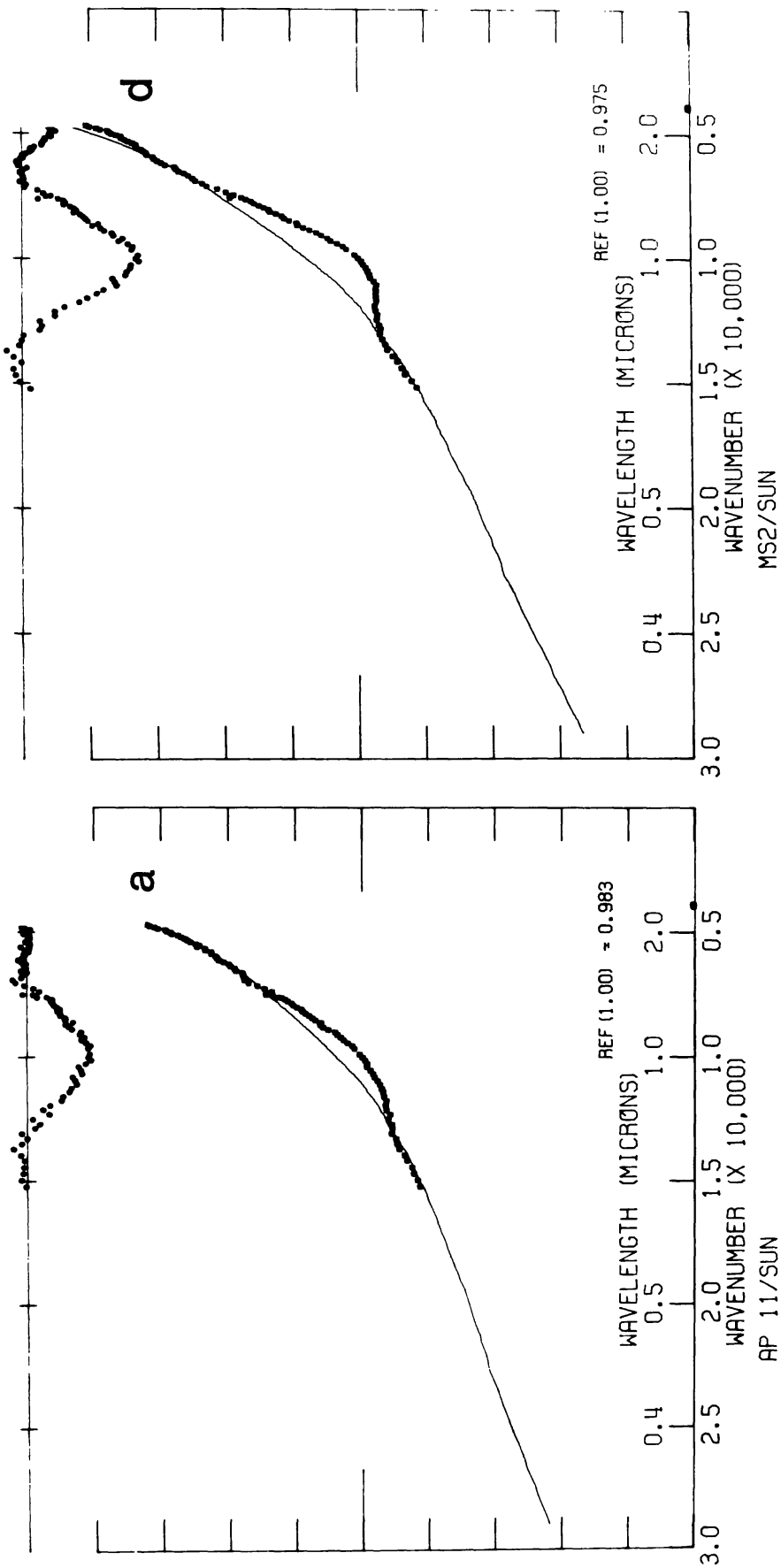

Fig. 4. Telescopic reflectance spectra *a* and *d* of Fig. 2 are plotted in energy units. A continuum is fit through the data at .73 and 1.5 μm. Shown above the spectra are residual absorption features after the continuum has been removed.

For some regions the IR imagery did not agree well with the photometry (spectra), with the estimated differences ranging up to 5%. Those cases, however, could generally be accounted for as particular observational or instrumental calibration difficulties (e.g., see IR discussion in Johnson *et al.*, 1977), allowing possibly erroneous data to be eliminated from consideration.

D. 2 μm band

An additional absorption feature can be seen near 2 μm in spectra *c* and *d* of Fig. 5. Since these data do not extend beyond 2.1 μm, the wavelength for the center of the 2 μm band cannot be estimated. It is clear that the 2 μm band is weaker than the 1 μm band and apparently absent for the darkest soils. Until further data are obtained, only the presence or absence of this weak 2 μm band can be determined for these five regions. A more thorough discussion of these preliminary lunar telescopic IR spectra can be found in McCord (pers. comm., 1978).

III. Unit Map of Mare Basalt Types

A summary of the usage of these four parameters for unit designation is listed in Table 1. It was found that almost all of the mare basalt types discerned in the .3 to 1.1 μm spectra by Pieters and McCord (1976) would have a unique unit designation with these four parameters and thus can be mapped relatively easily. It should

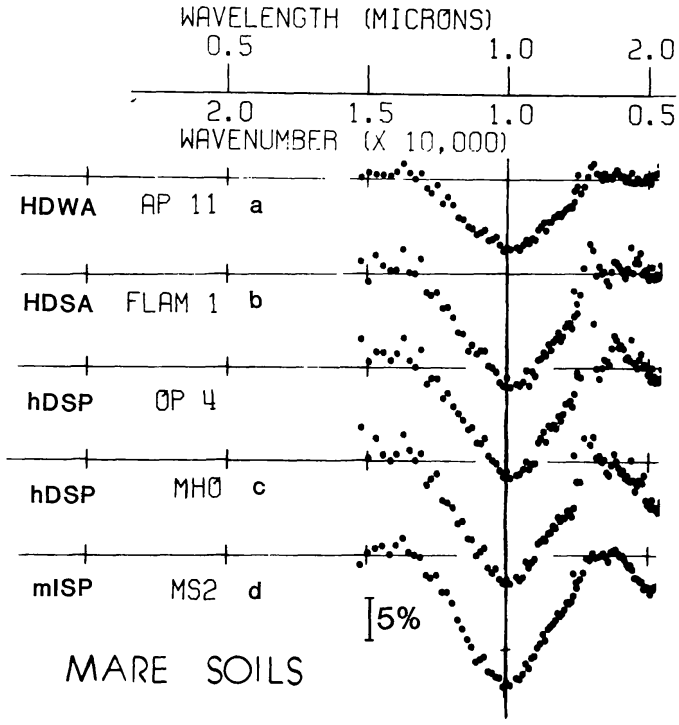

Fig. 5. Residual absorption features plotted in energy units after a continuum has been removed from each telescopic reflectance spectra of Fig. 2.

Table 1. Measurable parameters used to distinguish mare basalt types

Values	UV/VIS ratio (rel. to MS2)	Albedo (normal)	1 μm band	2 μm band
High	H: high (≳1.05)	B: bright (≳9.5%)	S: strong (e.g., MS2)	P: present (e.g., MS2)
·	h: med. high (1.02–1.05)	I: intermediate (8–9.5%)	G: general average (e.g., Ap 12)	
·	m: medium (.99–1.02)	D: dark (≲8%)	W: weak (e.g., Ap 11)	A: absent (e.g., Ap 11)
Low	L: low (≲.99)			– unknown (e.g., no data)

be noted again that subtle mineralogical differences, which require analysis of the nature of the 1 and 2 μm features, are lost in this classification scheme but will be investigated further in later studies when sufficient data are available.

A map of the regional distribution of mare basalt types as best discerned using the four parameters discussed above is shown in Fig. 6. The four-letter designation for each mare unit refers to the values of each parameter as itemized in Table 1. The overall regional extent of each unit is mapped without regard to small local variations. For complex areas where no dominant unit is apparent, the region is mapped as mottled (MOT). A more detailed examination of these mottled areas can be undertaken with sufficiently precise high resolution (~2 km) data.

Two additional types of volcanic material are also mapped. (1) MM: regions of extensive mantling material (Wilhelms and McCauley, 1971; Pieters *et al.*, 1973; Adams *et al.*, 1974; Pieters *et al.*, 1975; Zisk *et al.*, 1977), which presumably are pyroclastic deposits (Heiken *et al.*, 1974). Not all of these areas are alike; at least three different types of mantling material can be distinguished spectrally. (2) RS: areas of possible pre-mare volcanism in the highlands (Wood and Head, 1975; Head and Hess, 1978) which are distinctively red, or low in UV/VIS ratios (Malin, 1974; Head and McCord, 1978).

Assuming the distinctions between these basalt types are predominantly due to differences in chemical composition (see next section), a map can be constructed from Fig. 6 which illustrates the degree to which the current lunar samples are representative of lunar basalt chemistry. Shown in Fig. 7 are the basalt units from which samples have been obtained, those which are possibly similar to the sampled units, and those which are distinctively different from the sampled units. From this map it is evident that the existing lunar samples represent from ⅓ to ½ of the major basalt types on the surface of the moon. Until mare stratigraphy is further understood, no estimate can be made on how *volumetrically* well-sampled the lunar basalts are.

1978LPSC....9.2825P

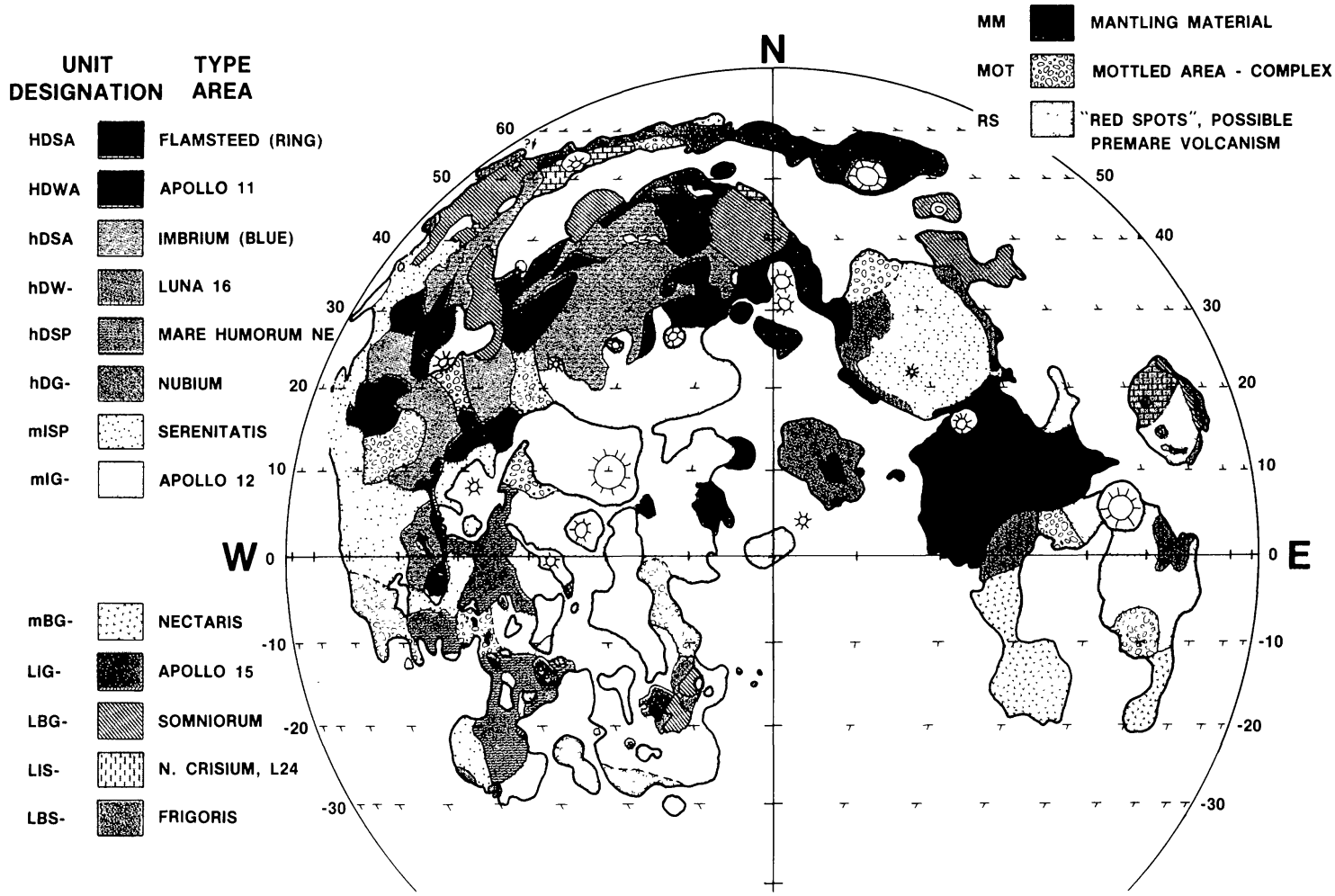

Fig. 6. Major basalt types for the front side of the moon as derived from the current spectral reflectance data. The letters used in unit designation refer to the values of measurable parameters listed in Table 1.

IV. Compositional Effects on Map Parameters

Variations in soil chemistry simultaneously affect all the parameters discussed above. Some parameters, however, are more sensitive than others to changes in particular chemical components. Discussed here are the major possible effects of composition on each separate parameter with an emphasis on those effects that can cause differences between maria. The interrelations between parameters and some of the techniques for interpreting this spectral information in a chemical context are discussed in the next section.

A. UV/VIS ratio

The UV/VIS ratio of lunar soil is determined by two types of competing phenomena: those that control the true absorption, or "color," of the surface particles and those that control the spectral contrast possible in reflected radiation. For mature soils with few mineral fragments the major contributor to the UV/VIS color is iron- and titanium-bearing glass with perhaps also an effect from finely dispersed Fe°. On the other hand, the spectral contrast in the UV is determined largely by the overall albedo.

UV Absorption. Homogeneous glasses occur as both individual fragments in soil as well as components of agglutinates. The spectral characteristics of various iron- and titanium-bearing synthetic glasses produced under controlled oxygen fugacity have been studied with transmitted light in detail by Bell *et al.* (1976) and with reflected light by Wells and Hapke (1977). The spectral properties of the lunar homogeneous glasses, such as a glass separate of an Apollo 11 soil (Adams, unpublished data), contain the same absorption features as the Fe-Ti glasses produced under controlled laboratory conditions. Various charge tranfer absorptions occur in the UV for these glasses involving Ti^{3+}, Ti^{4+}, and Fe^{2+} (Burns *et al.*, 1976; Bell *et al.*, 1976), creating a steep absorption edge from the visible into the ultraviolet. The slope of the UV absorption coefficient at .4 μm increases in a linear manner with the compositional product $FeO \cdot TiO_2$ (Bell *et al.*, 1976). In other words, the strength of the UV absorption is directly related to $FeO \cdot TiO_2$, the reflectance UV/VIS ratio is thus inversely related to $FeO \cdot TiO_2$, and non-opaque very iron- and titanium-rich glasses are very red. Recent experimental studies (Osborne *et al.*, 1978) have shown that the temperature of the surface may have an effect on the strength of these charge transfer absorptions, but that the effect would be minor for most lunar telescopic observations.

A possible second cause of absorption in the UV, and throughout the lunar continuum, is Fe° either as finely dispersed particles or as thin coatings (Hapke *et al.*, 1975; Gold *et al.*, 1977). Small particles of iron metal were observed in the first returned lunar soils (Agrell *et al.*, 1970). From magnetic and Mössbauer techniques, it was further shown (e.g., Housely *et al.*, 1973) that submicroscopic metal grains are enriched in mature soils. Precisely how submicron particles or coatings interact with light is poorly understood, but transmission spectra obtained by Bell and Mao (1977) of both an Apollo 16 agglutinate rich in submicroscopic Fe° and

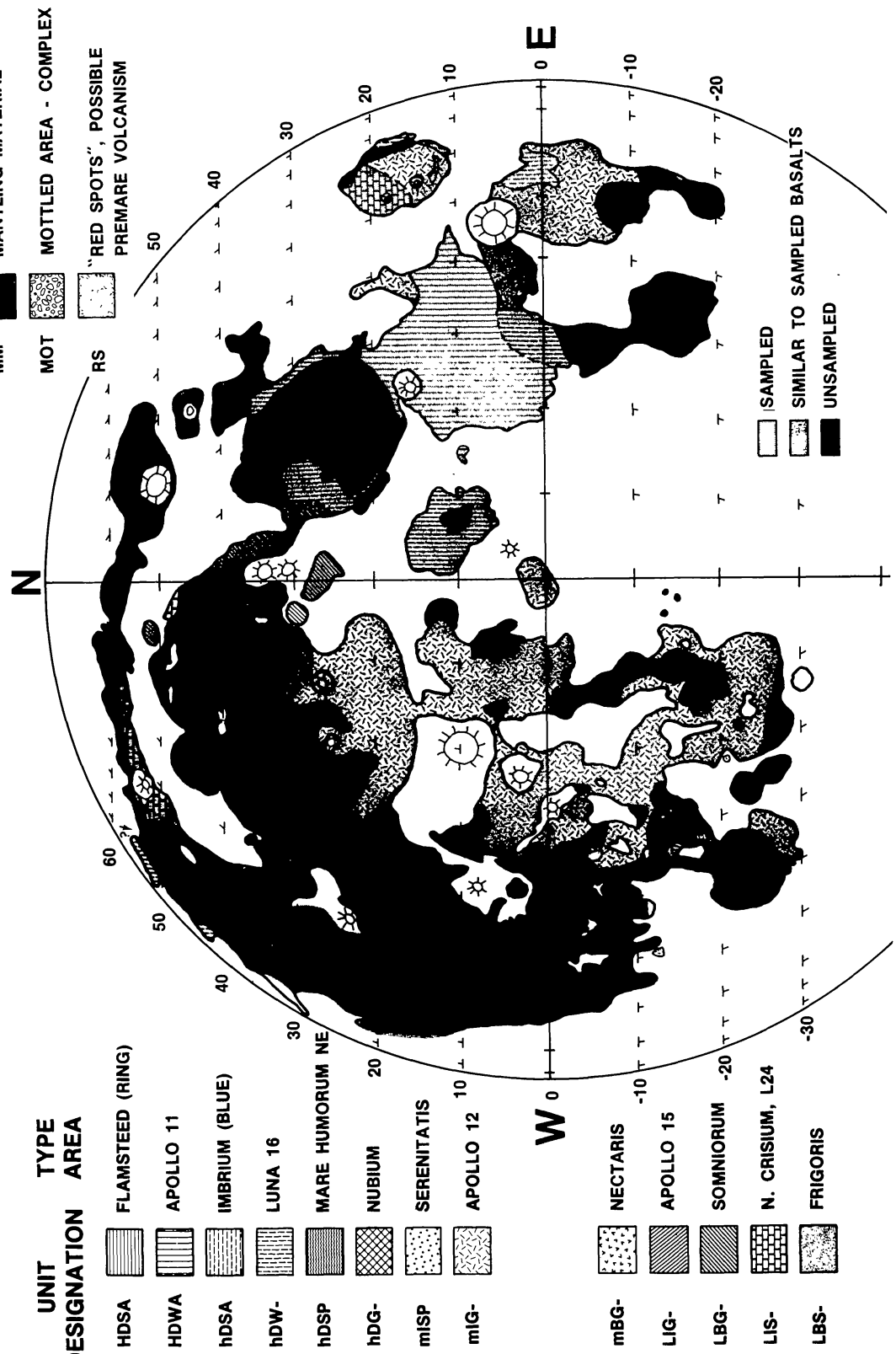

Fig. 7. Sampled and unsampled basalt types for the frontside of the moon as derived from figure 6. A color version of this figure appears as frontispiece plate #1.

thin (10–100Å) coatings of Fe° on transparent powders show a strong increase in absorbance toward the ultraviolet associated with the metal iron. Another, perhaps circumstantial, piece of evidence is the similarity of the reflectance of iron (Gaffey, 1976) to the average lunar soil continuum. In fact, the continuum used in Fig. 4 is the metal iron continuum of Gaffey.

Spectral Contrast. The degree to which an absorption feature can be observed in a reflectance spectrum is dependent on the overall spectral contrast of the surface material. Light must be able to get into and out of individual grains. At each particle interface light is either transmitted through the particle to emerge diffusely with imprinted absorption characteristics or specularly reflected (scattered) largely without spectral interaction. Although some specular reflection occurs at each interface, the amount of transmitted component is largely dependent on the opacity of the particles. Large differences in particle size and surface texture certainly affect the mean optical path length of light (specular and transmitted) interaction with surface particles (e.g., Adams and Filice, 1967). For mature undisturbed lunar soils, however, these physical parameters can be assumed roughly constant over the lunar surface leaving the mean optical path length of reflected radiation only a function of the general opacity of the surface particles and the relative proportions of the specular scatter and the diffuse (transmission) components.

Dark lunar soils have a relatively high specular component which can have a significant effect on the UV/VIS ratio (Pieters *et al.*, 1973). The far ultraviolet albedo measurements made of the moon can be used to estimate the amount of specular scatter assuming scatter is roughly independent of wavelength over the UV-VIS range. Lucke *et al.*, (1975) report the albedo of the moon to be about 3% at 1600 Å. Since silicates are essentially opaque at these wavelengths there can be no diffuse transmission component, and this measurement is essentially one of the specular scatter.

The effect of this relatively large component of specular scatter for dark soils at longer wavelengths is to lower the spectral contrast of any absorption feature. For example, if a soil has a strong absorption in the UV such that its UV/VIS ratio should be .5, its observed color will be 25–35% weaker due to the specular component, the amount depending on its albedo. This effect is itemized in Table 2 for three fictitious mare areas A, B, and C with 12, 10 and 8% observed albedo at .56 μm respectively. When 3% estimated scatter is accounted for in the VIS (.56 μm) and the UV (.40 μm), the observed UV/VIS color is weaker and different for each area (.625, .65 and .6875). The differences in albedo over the range observed on the moon can thus cause a "false" UV/VIS color difference between lunar areas of about 10%, which is simply the result of differences in spectral contrast.

As the VIS albedo is reduced spectral contrast in the UV is reduced. There is thus an inverse relation between the UV/VIS ratio and albedo. The darkest soils can be observed to be relatively blue due to the effect of albedo on spectral contrast. Their 'true' color, which contains the effects of composition may only be a secondary effect in the color measurement.

Table 2. Effects of nonspectral scattering on UV/VIS ratio

Spot	R(.56)	Est. Scatter	$R_0(.56)$	"true color" $R_0(.40)/R_0(.56)$	$R_0(.40)$	R(.40)	"observed color" R(.40)/R(.56)
A	12	3	9	.5	4.5	7.5	.625
B	10	3	7	.5	3.5	6.5	.65
C	8	3	5	.5	2.5	5.5	.6875

$R(\lambda)$ = observed reflectance
$R_0(\lambda)$ = pure diffuse reflectance (transmitted component)

B. Albedo

A number of competing hypotheses have been proposed which can explain the darkness of lunar soils. Some have to do with bulk chemistry and others have to do with the effects of maturation on the more mafic components (Fe, Ti). Most of the proposed processes could have a significant effect on the albedo of the lunar maria. The more interesting question, however, is which effects result in *variations* of overall albedo that can be measured and interpreted. It is not necessarily true that the strongest effect on albedo exhibits the most variability.

The overall difference in brightness between the bright highlands and the darker maria is due to a primary difference in mineralogy (higher feldspar content in the highlands) as is globally evidenced by the correlation between remote Al/Si measurements and albedo (Adler *et al.*, 1972; 1973). The proportion of relatively nonabsorbing plagioclase clearly has a direct effect on albedo. For the mare basalts currently sampled, plagioclase is a significant, but not dominant mineral phase (e.g., Papike *et al.*, 1976). Variations in plagioclase content play a secondary role to the variations seen in the more absorbing pyroxenes and opaques. Except for mare areas with extensive highland contamination it is likely that major variations in albedo for the maria are dominated by the differences that result from maturation of the mafic components.

As a soil is formed from mare basalts, changes in mineralogy occur. The surface is repeatedly crushed, fractured, melted, welded, and irradiated. With time 60 to 80% of the material is gradually transformed into the multi-component dark agglutinates characteristic of lunar soils. The darkness of these agglutinates dominates the albedo of the soil (Adams and McCord, 1973) but the agglutinates themselves are poorly understood and difficult to model. Contributions to the darkness of the agglutinitic soil can come from at least three sources: Fe-Ti glasses, Fe°, and opaques.

Fe-Ti glasses. The term "glasses" is used here to refer to the translucent amorphous glasses that occur individually as fragments and droplets in soils and that are a translucent component of agglutinates. Since Fe-Ti glasses are generally darker than a basalt powder of equivalent composition, their presence in lunar soils contributes to some extent to the overall darkening of lunar soil with time (Adams

and McCord, 1971). Most photographs and maps of visible albedo (obtained at .55 μm) could be affected by variations in the glass absorption edge (a function of $FeO \cdot TiO_2$) discussed previously. However, it is important to note that all the various Fe and Ti glasses have almost the same absorption coefficient between .62 and .65 μm except for extreme compositions (Bell *et al.*, 1976). For albedo maps produced near this wavelength range the effects of a given proportion of Fe-Ti glass on the absolute albedo would thus be the same for almost any glass composition; i.e., the composition of the Fe-Ti glass in a soil should have no effect on the albedo at .62–.65 μm. The .62 μm albedo map of Evsyukov and Barabashov (1973c) is distinct from those produced at shorter wavelengths, but nevertheless shows strong differences in albedo for the maria. It is thus inferred that there must be effects on the albedo of mature soils other than those due to glass composition to account for the observed variations at .62 μm.

Fe°. As mentioned in the previous section the presence of small quantities of metallic iron, either as finely dispersed particles or as thin coatings, may have an effect on the overall lunar continuum. Hapke *et al.* (1975) propose that the principal darkening effect for lunar soils is the submicroscopic Fe° formed in impact events and solar wind sputtering. An apparent correlation of Fe and Ti on the surfaces of soil particles led Gold *et al.* (1977) to a similar conclusion although there is also counter-evidence for no strong enrichment of Fe on the surface of particles (Housley and Grant, 1976). Nevertheless, it is possible, if not probable, that metallic iron contributes to the darkening of lunar soils with maturation.

For mature mare soils, however, it is unlikely that variations in soil *chemistry* will have significant effect on the degree of darkening due to metallic iron content. In a careful study of the magnetic properties of lunar soils, Morris (1978) was able to estimate the quantities of initial metallic iron, the amount of excess metallic iron of meteoritic origin, and the amount of excess metallic iron produced in the regolith by FeO reduction during meteoritic impact. Each of these three types of metallic iron contributes significantly to the total in a mature mare soil and together average about .8% by weight. The only component that depends much on the composition of the surface is the reduced excess metal which varies only about .1% Fe° for mature mare soils over a FeO range from 16 to 20%. However, the Apollo 11 soils, which were obtained from one of the darkest mare regions, are not significantly enriched in FeO nor reduced metal relative to the other returned mare soils. It is thus unlikely that the small differences in soil Fe° that result from differences in bulk FeO content account for the observed differences in albedo of mature mare surfaces.

Opaques. Lunar agglutinates contain various forms of opaques as mineral fragments, devitrified glass, and large amounts of unresolvable opaques. The reduced iron discussed separately above is also a component of soil opaques. The opaque lunar oxides identified in basalts (ilmenite, armalcolite) contain high and almost equal values of iron and titanium. The absolute amount of such oxides that occur in an agglutinitic soil cannot be easily determined but the relative proportion, including mineral fragments and submicroscopic particles, would be expected to be dependent on the amount of iron and titanium in the basalt regolith. Precisely how

the FeO or TiO_2 content of lunar soil controls the formation of submicroscopic opaques is not understood, but if it parallels the known lunar oxides, Ti plays a role at least equivalent to Fe. Thus, it seems to follow that the more iron- and titanium-rich a soil, the denser the total opaques, and the lower the overall albedo. Since FeO varies only approximately 25% in the returned lunar soils and TiO_2 (which is always less than ½ the amount of FeO) varies a factor of 10, TiO_2 content is expected to be directly responsible for much variation in the density of agglutinitic opaques and thus albedo.

C. 1 μm band

A variety of components found in the lunar soil contain absorption features near 1 μm due to Fe^{2+} in sixfold coordination (e.g., see Burns, 1970 or Adams, 1974). Listed in approximate decreasing influence these include: homogeneous glass, pyroxenes, olivine, and plagioclase. The homogeneous lunar glasses contain a broad, symmetric Fe^{2+} electronic transition absorption centered near 1.05 μm. The depth of this band in pure glass[1] is directly related to the FeO content (Bell *et al.*, 1976). The minimum of the 1 μm band of common lunar pyroxenes is coordinated with the 2 μm pyroxene band and ranges in wavelength from about .91 to .98 μm as a function of chemistry (Adams, 1974; Hazen *et al.*, 1978). The pyroxene Fe^{2+} band is more narrow than the glass band. Olivines contain a single nonsymmetric broad band centered between 1.03 and 1.06 μm (see Adams, 1975). Since olivine is weakly absorbing relative to the glasses and pyroxenes, any contribution from a minor olivine component in lunar soils is easily masked by the more absorbing materials. Lunar anorthositic plagioclase, with <1% FeO, exhibits a broad absorption with a band center that varies between 1.25 and 1.30 μm as a function of anorthite content (Adams and Goullaud, 1978). This plagioclase band, which can contribute an inflection to the long wavelength end of a 1 μm absorption, is rarely seen in lunar mare soils since it is weak and usually masked by stronger absorptions.

The weak feature seen near 1 μm in the spectra of Fig. 1-5 is a composite band most likely due to glass and pyroxene absorptions (Adams, pers. comm., 1978). The depth of the band is directly related to the relative proportion of components that contain 1 μm absorption bands. As mentioned above, in glasses the depth is also related directly to the FeO content. Perhaps the most important factor in interpretation of the depth of the observed band in soils, however, is the degree to which the band has been masked by the agglutinitic opaques of mature soils (Adams and Ralph, 1978).

[1]Recently a new kind of lunar glass has been discovered in the Luna 24 samples that has absorption bands which mimic the orderly bands of pyroxenes (Bell *et al.*, 1978). The origin of these peculiar glasses has not been determined, but they seem to be unique to the Luna 24 site.

D. 2 μm band

The only mineralogical component of lunar soils that contains a significant band near 2 μm is pyroxene (see Adams, 1974, 1975). (Iron-bearing glasses exhibit a broad weak feature near 1.8 to 2.0 μm that is difficult to distinguish from a continuum.) The depth of the 2 μm pyroxene band is directly related to the proportion of pyroxenes remaining in the soil and inversely related to the degree of masking by opaques.

V. Synthesis and Interpretation

A summary of the possible effects of composition on the measurable spectral parameters used in this study is presented in Table 3. From the previous discussion it is clear that no single parameter value can unambiguously provide chemical information for a given unsampled area. Sufficient data do exist, however, to eliminate some of the possibilities and to provide a reasonable estimate for some chemical information.

A. TiO_2

From spectra of returned soil samples it was noted by Charette *et al.* (1974) that an empirical relation exists between the TiO_2 content of the soils and the relative slope of the continuum in the unltraviolet, or UV/VIS ratio. This empirical relation has been used to estimate the % TiO_2 for unsampled regions and to predict the composition of Apollo 17 and Luna 24 soils from the UV/VIS ratio (Pieters, *et al.*, 1973, 1976). Although the choice of ground truth samples for verification is difficult, the predictions have been generally correct. (See Head *et al.*, 1978b, for a discussion of the Luna 24 soil.)

With a better understanding of the effects of compositional parameters on true color and albedo, a revised estimate of the effects of TiO_2 on the UV/VIS ratio can

Table 3. Effects of composition on measurable spectral parameters for mare soils

		1 μm band		2 μm band	
UV/VIS	Albedo (.62 μm)	Wavelength	Depth	Wavelength	Depth
1. In: glass UV absorption (In: $FeO{\cdot}TiO_2$)	1. D: % plag	1. glass	1a. D: FeO in glass 1b. D: % glass	1. px comp.	1. D: % px
2. In: Fe°	2. In: glass absorption	2. px comp.	2. D: % px		2. In: opaques (In: TiO_2,FeO)
3. In: Albedo	3. In: opaques (In: TiO_2,FeO) 4. In: Fe°	3. ol	3. D: % ol 4. In: opaques (In: TiO_2,FeO)		

In: inversely related
D: directly related
px pyroxene
ol olivine
comp composition

be made. Briefly, for the darkest mare soils the composition effects that control albedo and spectral contrast are responsible for the UV/VIS ratio; bright mare soils are more likely to allow some of the true color effects to be detected. The separation between albedo effects and true absorption in the UV for the average albedo mare soil cannot be made completely without additional data. Shown in Fig. 8 is the revised estimate for the relation between UV/VIS ratio and % TiO_2. Selected mature mare soils provide the ground truth data. Shown above the figure is the range of .40/.56 μm values for each of the basalt types discerned by the spectral data. Heavy lines are used for unsampled basalt units. The possible range of TiO_2 for these basalts can be estimated from the stippled area on the chart.

Mature Ti-rich soils contain abundant opaque agglutinates. High-Ti soils will thus be very blue due simply to the low spectral contrast. To what degree very blue soils will also be Ti-rich cannot be precisely determined without samples. Note, however, that all the blue basalt types (high in UV/VIS ratio) are also the darkest mare soils. All the evidence we currently have from laboratory studies on lunar

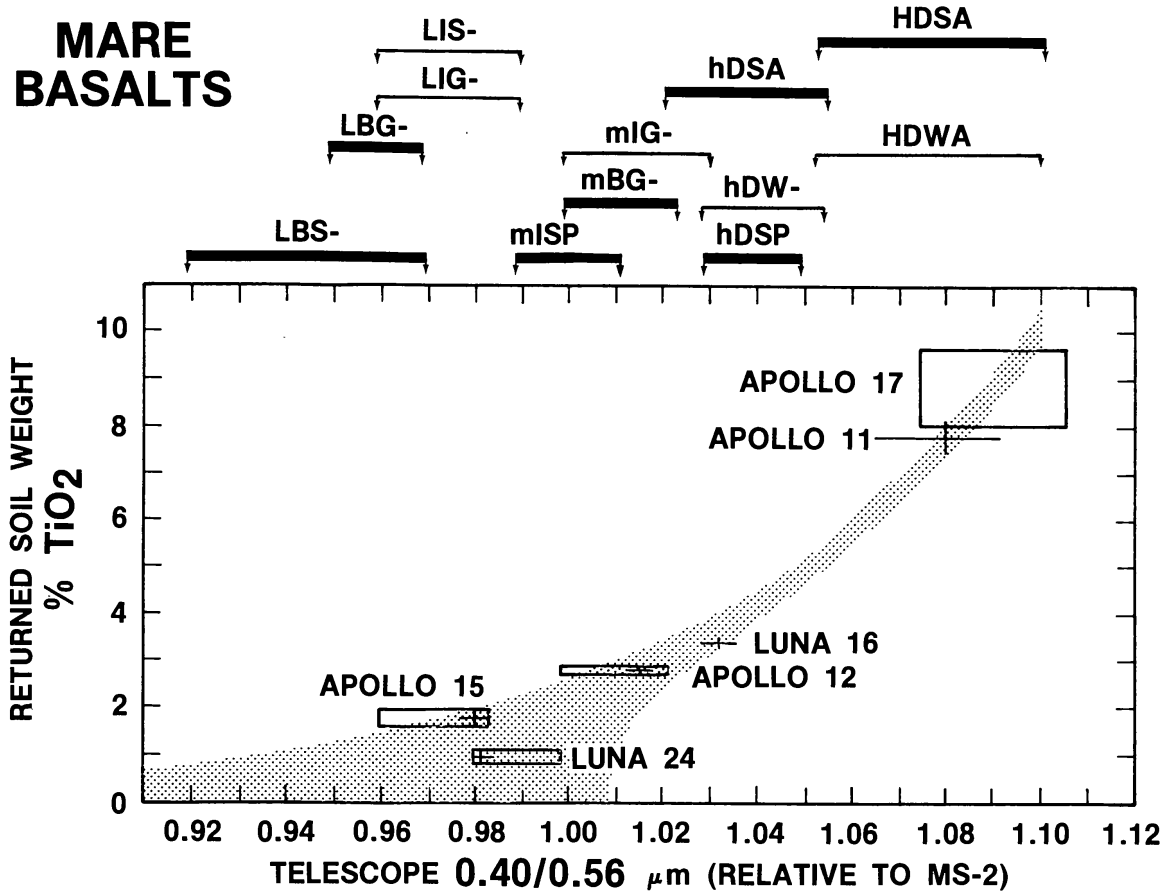

Fig. 8. Relationship between wt % TiO_2 in lunar mare soils and the .40/.56 μm reflectance ratio for telescopic spectra relative to MS2 (after Charette *et al.*, 1974 and Pieters and McCord, 1976). The stippled area is the estimated range of TiO_2 that can be derived from a .40/.56 μm ratio measurement of mature mare regions. Shown above the plot are the ranges of .40/.56 μm ratio observed for each of the basalt types discussed in this paper. The heavy lines indicate unsampled basalt types.

soils and lunar analogues indicates that unless there is some unsuspected process at work in the unsampled areas, the very dark *and* blue mare basalts must also be very titanium-rich. Fe° may contribute to the opaques, but the darkness of the soil is largely controlled by the Ti-Fe phases.

In a similar manner bright and intermediate albedo mare soils contain fewer Ti-Fe absorbing phases and thus must be lower in titanium. The relation between UV/VIS ratio and albedo is not simple, however. Once some of the opaque phases are removed, the relative effects of other components on albedo and color can be stronger. In particular, the combination of titanium and iron has the effect of either raising or lowering the UV/VIS ratio depending on whether the opaques or the homogeneous glasses play a dominant role. From the empirical evidence, opaques are expected to lose control of the UV/VIS ratio for mare soils when there is less than about 4% TiO_2. Below this value plagioclase and Fe° content and homogeneous glass composition can have a stronger effect on the UV/VIS ratio and albedo. For the reddest and brightest mare basalts (LBG- and LBS-) it is reasonable to estimate a very low TiO_2 content ($\lesssim$1.5%). For basalts with a .40/.56 μm relative ratio between about .96 and 1.01, however, the TiO_2 content could be anything from medium-low to very low.

B. FeO

Although there is no simple parameter that can be used to estimate the FeO content for mature soils, the strength of the 1 μm glass band has been the most fruitful (Charette *et al.*, 1977; Adams and Ralph, 1978 and pers. comm.). If a few requirements are met, relative FeO content can be estimated for a few cases from the depth of the 1 μm band. (1) The degree of masking (by opaques) must be held constant. (2) The relative proportion of homogeneous glasses in a mature soil must be constant. (3) The relative contribution of pyroxene and olivine do not change. The first requirement is likely to be met for those basalt types that have both the same albedo and UV/VIS ratio. The second requirement would have to come from an assumption that the regolith formation process is the same everywhere and effectively independent of original composition. The third requirement could be met by those basalt types that have the same 2 μm (pyroxene) characteristics. A few basalt types to be discussed below (e.g., HDSA and mISP) meet these requirements relative to sampled basalts and are likely to be high iron.

C. Specific unsampled basalt types

HDSA. The unsampled high-Ti (dark and blue) basalts of the western nearside in Oceanus Procellarum (HDSA) and Mare Imbrium (hDSA) are distinct from those of the Eastern maria (HDWA) in both age and spectral character. Since the HDSA basalts are only slightly bluer (and often darker) than the hDSA basalts, and the two units frequently occur together, they can probably be considered as two subgroups of the same basalt type. These western basalts, which were emplaced relatively late for mare volcanism (Boyce, 1976), exhibit a much stronger

1 μm feature than the earlier eastern basalts (Pieters, and McCord, 1976). In UV/VIS ratio, .62 μm albedo, and 2 μm characteristics the eastern HDWA basalts of Apollo 11 and 17 are essentially identical to the western HDSA basalts near Flamsteed. They both are relatively blue, very dark, and without a noticeable 2 μm band. The structure of the 1 μm band for these two basalt types is similar—asymmetric and centered beyond 1 μm—but the band for HDSA is almost twice as strong as the band for HDWA (Fig. 5). The spectral contrast or degree of masking for the two types of basalt is not likely to be different because of the similarity of the UV/VIS ratio and the albedo. Thus spectral contrast cannot account for the difference in band depth. Since neither show evidence of a major pyroxene contribution in the 2 μm region, the difference at 1 μm must be due to something other than pyroxene content, e.g., Fe-Ti glass. Similarly, since the center of the 1 μm feature for both basalt types lies beyond 1 μm, the feature is likely to be dominated almost entirely by the glass band. There are two possible interpretations. (1) HDSA soil contains proportionally *more* glass than HDWA or (2) the composition of the HDSA glass, and thus the bulk soil, is richer in FeO than HDWA.

If the first possibility is true, then the cumulative soil formation process does not result in the same proportions of glasses for all mare surfaces. It is not known whether the composition of the surface can significantly affect the amount of *glass* produced during soil formation. Adams *et al.* (1975) have shown that the bulk composition apparently does affect the amount of *agglutinates* formed in a mature soil. Alternatively, for some undetermined reason the original basalt surface could have been significantly more glassy than those for which samples have been returned, and the resulting soil maintains the glass enrichment. Whatever process is in operation must, nevertheless, apply equally over the large areal extent of these HDSA and hDSA basalts.

The second possiblity is perhaps the more enticing, with the bulk HDSA soil being enriched in FeO relative to the Apollo 11 HDWA soil. If it is safe to assume that the relative proportions of non-opaque glass in the western HDSA and eastern HDWA soils are equivalent and the making components are the same, then the stronger 1 μm band of HDSA can be directly interpreted as indicating more FeO. A more detailed understanding of the effects of masking on a glass absorption band are required to quantify this effect. In either case, the HDSA basalts, and the related hDSA basalts, are clearly different from anything that has been sampled.

hDSP. A second type of unsampled young basalt occurs in the western maria and is moderately titanium-rich. Found in NE Mare Humorum and SE Oceanus Procellarum, hDSP basalts are as dark as the Eastern Luna 16 basalts (hDW-) and almost as dark as Mare Tranquillitatis. Throughout the spectral range .3 μm to .90 μm the hDSP basalts are very similar to the hDSA Imbrium basalts. Some important distinctions in the 1 μm and 2 μm regions, however, can be made between these two types of medium high-Ti western basalts. Although the 1 μm band is strong (this distinguishes them both from the eastern basalts) small differences in the structure between .9 μm and 1.1 μm can be seen in the spectra for hDSP and hDSA in Fig. 3. The full structure of the band can be seen in better detail in Fig. 5. In comparison with HDSA, the spectrum of hDSP exhibits a more narrow 1 μm

band that is centered at a shorter wavelength. The spectrum for hDSP also contains a 2 μm band. The hDSP spectra clearly show less of the glass feature seen in HDSA and hDSA spectra. The soils for hDSP are thus likely to be much more pyroxene-rich than either of the other medium- high-Ti basalt types and are thus another distinct type of basalt that has not been sampled.

mISP. Central Mare Serenitatis has long been used as a standard area for telescopic studies. Its intermediate albedo and average UV/VIS ratio indicate mISP is a low titanium basalt, but one for which the spectral calibration is not sufficiently precise to determine whether it is a very low-Ti basalt (VLT). Although many other low-Ti regions have similar spectral properties, the Serenitatis mISP basalts are spectrally distinct and exhibit a slightly stronger 1 μm absorption feature than the others. Even though mISP contains the strongest 1 μm band in Fig. 5, the depth of the feature cannot be compared directly to the other spectra since the spectral contrast is likely to be different from the darker basalts. Similarly, the 2 μm absorption band for mISP in Fig. 5 indicates a pyroxene component, but implies nothing concerning its relative proportion. The presence of the 2 μm band may simply be due to the increase in spectral contrast with lighter soils. It is more appropriate to compare mISP with similar basalts such as mIG- and mBG-. The only 1 μm data that exist are the .3 to 1.1 μm spectra such as those in Fig. 3; it can be noted that mISP has a slightly stronger 1 μm feature when compared to other basalts with similar albedo and UV/VIS ratio. There can be three possible interpretations for the strong 1 μm band: (1) mISP contains FeO-rich glass, i.e., the bulk composition is FeO-rich; (2) mISP is pyroxene-rich; or (3) mISP is glass-rich. Although without additional IR data there is no way to distinguish among these possibilities, the first (FeO-rich) interpretation is also consistent with the high iron values found over Mare Serenitatis in the recently analyzed gamma-ray orbital data (Arnold *et al.*, 1978).

Central Serenitatis mISP basalts have been suggested as a possible source material for the VLT basalts discovered as minor components in the Apollo 17 drill core (Vaniman and Papike, 1977). There are two other possible VLT source candidates in the region, LBG- and LIG-, that occur along the northern edge of the Serenitatis basin in Somniorum and in eastern Le Monnier respectively and could be present elsewhere as a subsurface basalt. Since the Apollo 17 VLT basalts have a relatively high feldspar component (possibly affecting albedo) and are not particularly iron-rich nor particularly enriched in pyroxene, the LBG- basalts are a slightly better candidate than the others for being the associated basalt type. A sample from central Serenitatis mISP would provide an ideal piece of ground truth for the orbital and telescopic remote sensing studies.

VI. Summary and Future Work

Presented here is a nearside map of the various lunar basalt types that can be identified using the currently available remotely sensed spectral reflectance data for lunar soils. The relative slope of the lunar continuum (UV/VIS ratio), the albedo, and the general nature of the 1 μm and the 2 μm absorption features are used

to distinguish 13 distinct basalt types. Spectra of small regions are used to identify and quantify spectral features of each distinct unit whereas multispectral imagery is used to define and map the extent of units. Regions which are likely to be similar to sampled basalts are identified by their spectral properties. The areal extent of basalts which are distinctly different from those sampled includes about ⅔ of the nearside maria. Most of these unsampled basalt types occur in the western maria.

Background laboratory studies on lunar, terrestrial and synthetic material provide a basis for a partial interpretation for some of the unsampled basalt regions. As more telescopic data accumulate, some of the unit designations and/or boundaries may change slightly, but the general framework of the information will not. There are simply a large number of major units on the lunar surface for which no similar samples exist in the Luna or Apollo collections. Clearly needed is more information on the chemistry and mineralogy of the various types of surface material. Much information will be obtained from continuing telescopic and laboratory studies in the near-infrared. The precision, spectral range, and spatial coverage and resolution that can only be obtained with spacecraft measurements, however, are required for major advances in exploration of our nearest neighbor.

Acknowledgments—I wish to acknowledge the many fruitful discussions with Drs. Tom McCord and John Adams concerning lunar reflectance data and interpretations. They both contributed significantly in spirit to this manuscript. A number of people generously contributed unpublished reflectance data for this analysis: John Adams, Torrence Johnson, Dennis Matson, Tom McCord, and Ewen Whitaker. This paper is the result of work done as part of the LPI Basaltic Volcanism Study Project and represents Basaltic Volcanism Contribution number 31.

REFERENCES

Adams J. B. (1974) Visible and near-infrared diffuse reflectance spectra of pyroxenes as applied to remote sensing of solid objects in the solar system. *J. Geophys. Res.* **79,** 4829–4836.

Adams J. B. (1975) Interpretation of visible and near-infrared diffuse reflectance spectra of pyroxenes and other rock forming minerals. In *Infrared and Raman Spectroscopy of Lunar and Terrestrial Materials* (C. Karr, ed.), p. 91–116. Academic Press, N.Y.

Adams J. B., Charette M. P. and Rhodes J. M. (1975) Chemical fractionation of the lunar regolith by impact melting. *Science* **190,** 380–381.

Adams J. B. and Filice A. L. (1967) Spectral reflectance 0.4 to 2.0 microns of silicate rock powders. *J. Geophys. Res.* **72,** 5705–5715.

Adams J. B. and Goullaud L. H. (1978) Plagioclase feldspars: Visible and near infrared diffuse reflectance spectra as applied to remote sensing. *Proc. Lunar Planet. Sci. Conf. 9th.* This volume.

Adams J. B. and McCord T. B. (1971) Optical properties of mineral separates, glass, and anorthositic fragments from Apollo mare samples. *Proc. Lunar Sci. Conf. 2nd*, p. 2183–2195.

Adams J. B. and McCord T. B. (1973) Vitrification darkening in the lunar highlands and identification of Descartes material at the Apollo 16 site. *Proc. Lunar Sci. Conf. 4th*, p. 163–177.

Adams J. B., Pieters C. and McCord T. B. (1974) Orange glass: Evidence for regional deposits of pyroclastic origin on the moon. *Proc. Lunar Sci. Conf. 5th*, p. 171–186.

Adams J. B. and Ralph R. L. (1978) Diffuse reflectance spectra of Luna 24 soils. In *Mare Crisium: The View from Luna 24*, (R. B. Merrill and J. J. Papike, eds.), p. 81–87.Pergamon, N.Y.

Adler I., Gerard J., Trombka J., Schmadebeck R., Lowman P., Blodget H., Yin L., Eller E., Lamothe R., Gorenstein P., Bjorkholm P., Harris B. and Gursky H. (1972) The Apollo 15 X-ray fluorescence experiment. *Proc. Lunar Sci. Conf. 3rd*, p. 2157–2178.

Adler I., Trombka J. I., Schmadebeck R., Lowman P., Blodget H., Yin L., Eller E., Podwysocki M., Weidner J. R., Bickel A. L., Lum R. K. L., Gerard J., Gorenstein P., Bjorkholm P. and Harris B. (1973) Results of the Apollo 15 and 16 X-ray experiment. *Proc. Lunar Sci. Conf. 4th*, p. 2783–2791.

Agrell S. O., Scoon J. H., Muir I. D., Long J. V. P., McConnell J. D. C. and Peckett A. (1970) Observations on the chemistry, mineralogy and petrology of some Apollo 11 lunar samples. *Proc. Apollo 11 Lunar Sci. Conf.*, p. 93–128.

Arnold R. J., Davis P. A. and Reedy R. C. (1978) Gamma ray maps of lunar titanium and iron (abstract). In *Lunar and Planetary Science IX*, p. 25–26. Lunar and Planetary Institute, Houston.

Bell P. M. and Mao H. K. (1977) Optical spectra of thin metallic coatings with application to the spectra of lunar soil samples (abstract). In *Lunar Science VIII*, p. 80–90. The Lunar Science Institute, Houston.

Bell P. M., Mao H. K., Hazen R. M. and Mao A. L. (1978) The Luna 24 sample from Mare Crisium: New structural features in lunar glasses deduced from a study of crystal-field spectra. In *Mare Crisium: The View from Luna 24*, (Merrill R. B. and J. J. Papike, eds.), p. 265–280. Pergamon, N.Y.

Bell P. M., Mao H. K. and Weeks R. A. (1976) Optical spectra and electron paramagnetic resonance of lunar and synthetic glasses: A study of the effects of controlled atmosphere, composition, and temperature. *Proc. Lunar Sci. Conf. 7th*, p. 2543–2559.

Boyce J. M. (1976) Age of flow units in the lunar nearside maria based on Luna Orbiter IV photographs *Proc. Lunar Sci. Conf. 7th*, p. 2717–2728.

Burns R. G. (1970) *Mineralogical Applications of Crystal Field Theory*. Cambridge Univ. Press, London. 224 pp.

Burns R. G., Parkin K. M., Loeffler B. M., Leung I. S. and Abu-Eid R. M. (1976) Further characterization of spectral features attributable to titanium on the moon. *Proc. Lunar Sci. Conf. 7th*, p. 2651–2578.

Charette M. P., McCord T. B., Pieters C. and Adams J. B. (1974) Application of remote spectral reflectance measurements to lunar geology classification and determination of titanium content of lunar soils. *J. Geophys. Res.* **79,** 1605—1613.

Charette M. P., Taylor S. R., Adams J. B. and McCord T. B. (1977) The detection of soils of Fra Mauro basalt and anorthositic gabbro composition in the lunar highlands by remote spectral reflectance techniques. *Proc. Lunar Sci. Conf. 8th*, p. 1049–1061.

Evsyukov N. N. and Barabashov N. P. (1973a) Color map of the visible hemisphere of the moon. Academy of Science, Kiev, USSR.

Evsyukov N. N. and Barabashov N. P. (1973b) Photometric map of the visible hemisphere of the moon. Academy of Science, Kiev, USSR.

Evsyukov N. N. and Barabashov N. P. (1973c) Albedo map of the visible hemisphere of the moon. Academy of Science, Kiev, USSR.

Frontispiece (1977) *Proc. Lunar Sci. Conf. 8th*, Vol. 1, Plate 7.

Gaffey M. J. (1976) Spectral reflectance characteristics of the meteorite classes. *J. Geophys. Res.* **81,** 905–920.

Gold T., Bilson E. and Baron R. L. (1977) The search for the cause of the low albedo of the moon *J. Geophys. Res.* **82,** 4899–4908.

Hapke B., Cassidy W. and Wells E. (1975) Effects of vapor deposition procession on the optical, chemical and magnetic properties of the lunar regolith. *The Moon* **13,** 339–353.

Hazen R. M., Bell P. M. and Mao H. K. (1978) Effects of compositional variation on absorption spectra of lunar pyroxenes. *Proc. Lunar Planet. Sci. Conf. 9th.* This volume.

Head J. W., Adams J. B., McCord T. B., Pieters C. and Zisk S. H. (1978b) Regional stratigraphy and geologic history of Mare Crisium. In *Mare Crisium: The View from Luna 24* (R. B. Merrill and J. J. Papike, eds.), p. 43–74. Pergamon, N.Y.

Head J. W. and Hess P. C. (1978) Geologic characteristics of lunar highland volcanic domes (Gruithuisen and Mairan region) and possible eruption conditions (abstract). In *Lunar and Planetary Science IX*, p. 488–490. Lunar and Planetary Institute, Houston.

Head J. W. and McCord T. B. (1978) Imbrian-age highland volcanism on the moon: The Gruithuisen

and Mairan Domes. *Science* **199,** 1433–1436.
Head J. W., Pieters C., McCord T. B., Adams J. B. and Zisk S. H. (1978a) Definition and detailed characterization of lunar surface units using remote observations. *Icarus* **33,** 145–172.
Heiken G. H., McKay D. S. and Brown R. W. (1974) Lunar deposits of possible pyroclastic origin. *Geochim. Cosmochim. Acta.* **38,** 1703–1718.
Housley R. M. and Grant R. W. (1976) ESCA studies of the surface chemistry of lunar fines. *Proc. Lunar Sci. Conf. 7th*, p. 881–889.
Housley R. M., Grant R. W. and Paton N. E. (1973) Origin and characteristics of excess Fe metal in lunar glass welded aggregates. *Proc. Lunar Sci. Conf. 4th*, p. 2737–2749.
Johnson T. V., Mosher J. A. and Matson D. L. (1977) Lunar spectral units: A northern hemispheric mosaic. *Proc. Lunar Sci. Conf. 8th*, p. 1013–1028.
Johnson T. V., Pieters C. and McCord T. B. (1973) Mare Humorum: An integrated study of spectral reflectivity. *Icarus* **19,** 224–229.
Lucke R. L., Henry R. C. and Fastie W. G. (1975) Far ultraviolet albedo of the moon from Apollo 17 (abstract). In *Lunar Science VI*, p. 528–530. The Lunar Science Institute, Houston.
Malin M. C. (1974) Lunar red spots: Possible pre-mare materials. *Earth Planet Sci. Lett.* **21,** 331–341.
McCord T. B. (1968) Color differences on the lunar surface. PhD. Dissertation, California Institute of Technology, Pasadena. 181 pp.
McCord T. B. (1969) Time dependence of lunar differential color *Astron. J.* **74,** 273–278.
McCord T. B., Grabow M., Feierberg M. A., MacLaskey D. and Pieters C. (1978) Lunar multispectral maps: Part II of the lunar nearside. Submitted to *Icarus*.
McCord T. B., Pieters C. and Feierberg M. A. (1976) Multispectral mapping of the lunar surface using ground-based telescopes. *Icarus* **29,** 1–34.
Morris R. V. (1978) Reduction excess, meteoritic excess, and initial metals in lunar soils: Origins of the excess metal. *Earth and Planet Sci. Lett.* In press.
Osborne M. D., Parkin K. M. and Burns R. G. (1978) Temperature dependence of Fe-Ti spectra in the visible region: Implications to mapping Ti concentrations of hot planetary surfaces. *Proc. Lunar Planet. Sci. Conf. 9th.* This volume.
Papike J. J., Hodges F. N. and Bence A. E. (1976) Mare basalts: Crystal chemistry, mineralogy, and petrology. *Rev. Geophys. Space Phys.* **14,** 475–540.
Pieters C. (1977a) Characterization and distribution of lunar mare basalt types using remote sensing techniques. Ph.D. dissertation, Massachusetts Institute of Technology, Cambridge, Massachusetts. 348 pp.
Pieters C. (1977b) Characterization of lunar mare basalt types-II: Spectral classification of fresh mare craters. *Proc. Lunar Sci. Conf. 8th*, p. 1037–1048.
Pieters C., Head J. W., McCord T. B., Adams J. B. and Zisk S. (1975) Geochemical and geological units of Mare Humorum: Definition using remote sensing and lunar sample information. *Proc. Lunar Sci. Conf. 6th*, p. 2689–2710.
Pieters C. and McCord T. B. (1976) Characterization of lunar mare basalt types: I. A remote sensing study using reflection spectroscopy of surface soils. *Proc. Lunar Sci. Conf. 7th*, p. 2677–2690.
Pieters C., McCord T. B. and Adams J. B. (1976) Regional basalt types in the Luna 24 landing area as derived from remote observation. *Geophys. Res. Lett.* **3,** 697–700.
Pieters C., McCord T. B., Zisk S. and Adams J. B. (1973) Lunar black spots and nature of the Apollo 17 landing area. *J. Geophys. Res.* **78,** 5867–5875.
Pohn H. and Wildey R. L. (1970) A photoelectric-photographic study of the normal albedo of the moon. *U.S. Geol. Survey Prof. Paper (map) 599-E.*
Soderblom L. A. (1970) The distribution and ages of regional lithologies in the lunar maria. Ph.D. dissertation, California Insitute of Technology, Pasadena. 139 pp.
Vaniman D. T. and Papike J. J. (1977) Very low Ti (VLT) basalts: A new mare rock type from the Apollo 17 drill core. *Proc. Lunar Sci. Conf. 8th*, p. 1433–1471.
Wells E. B. and Hapke B. (1977) Lunar soil: iron and titanium bands in the glass fraction. *Science* **195,** 977–979.
Whitaker E. A. (1972) Lunar color boundaries and their relationship to topographic features: A prelim-

inary survey. *The Moon* **4,** 348–355.

Wilhelms D. E. and McCauley J. (1971) Geologic map of the near side of the moon. U.S. Geol. Survey Misc. Geol. Inv. Map I-703.

Wood C. A. and Head J. W. (1975) Geologic setting and provenance of spectrally distinct pre-mare material of possible volcanic origin. *Origin of Mare Basalts*, p. 189–193. The Lunar Science Institute, Houston.

Zisk S. H., Hodges C. A., Moore H. J., Shorthill R. W., Thompson T. W., Whitaker E. A. and Wilhelms D. E. (1977) The Aristarchus-Harbinger region of the moon: Surface geology and history from recent remote sensing observations. *The Moon* **17,** 59–99.